Clays and Clay Minerals, Vol. 48, No. 6, 665–681, 2000.

MOLECULAR DYNAMICS SIMULATIONS OF THE ADSORPTION OF METHYLENE BLUE AT CLAY MINERAL SURFACES

CHING-HSING YU,[1] SUSAN Q. NEWTON,[1] MYA A. NORMAN,[1] DAVID M. MILLER,[2] LOTHAR SCHÄFER,[1] AND BRIAN J. TEPPEN[3]

[1]Department of Chemistry, University of Arkansas, Fayetteville, Arkansas 72701 USA
[2]Department of Crop, Soil, and Environmental Sciences, University of Arkansas, Fayetteville, Arkansas 72701 USA
[3]Department of Crop and Soil Sciences, Michigan State University, East Lansing, Michigan 48824-1325 USA

Abstract—Molecular dynamics simulations were performed of the adsorption of methylene blue (MB) on model beidellite, montmorillonite, and muscovite mica surfaces, using a previously determined empirical force field developed for dioctahedral clays. The simulations show that the adsorption of MB on mineral surfaces can result in a variety of configurations, including single and double layers of MB parallel to the basal surface, and irregular clusters. The $d(001)$ values of ~12.3 and ~15.7 Å are assigned to dry phases with parallel single and double layers of MB, respectively, in agreement with X-ray studies. At intermediate MB loadings, stacks inclined to basal surfaces are formed. The stacks of MB ions inclined by 65–70° relative to the (001) plane of muscovite are not found on dry surfaces, in contrast to previous studies. Configurations similar to those proposed by others form spontaneously in the presence of H_2O, but the ions in the model systems are not quite as ordered and not ordered in exactly the same way as the ones previously described, and they display a mobility that is not compatible with strict atomic order. The formation of a triple layer of H_2O interspersed with ions may occur in the interlayer. Overall, the results of the simulations confirm that the MB-ion method must be used with great caution in surface-area determinations, because of the multiplicity of possible configurations. At the same time, the ability for adsorption to occur as either single or multiple MB layers is useful to determine cation-exchange capacity over a wide range of surface-charge densities.

Key Words—Adsorption of Methylene Blue, Clay Cation-Exchange Capacity Determination, Clay Surface-Area Determination, Molecular Dynamics Simulations.

INTRODUCTION

Methylene blue (MB) has been used to characterize clays for more than 60 years (for a review see Lagaly, 1981). In 1970, systematic methods were developed (Brindley and Thompson, 1970; Hang and Brindley, 1970), which use MB adsorption to determine both surface areas and cation-exchange capacities (CEC) of clay minerals. The latter are estimated from the plateaus of adsorption isotherms, whereas the former are deduced from the flocculation behavior of clays suspended in MB solutions. For cation-exchange determinations, inorganic cations are usually assumed to be fully exchanged by MB.

The interest in MB adsorption is part of a general interest in the interactions of organic cationic dye molecules with clay surfaces, prompted by the utility of aqueous suspensions of clay minerals in various applications, such as in agriculture, catalysis, and decontamination (Arbeloa *et al.*, 1997; Chu and Johnson, 1979; Breen and Loughlin, 1994; De *et al.*, 1973, 1974; Fischer *et al.*, 1998; Garfinkel-Shweky and Yariv, 1997a, 1997b; Mishael *et al.*, 1999; Neumann *et al.*, 1996; Rytwo *et al.*, 1996, 1998; Saehr *et al.*, 1978; Schramm *et al.*, 1997; Schoonheydt, 1994). In addition, MB adsorption was studied in connection with pharmaceutical projects (Viseras and Lopez-Galindo, 1999), clay swelling (Xeidakis, 1996a, 1996b) and the characterization of cement materials (Bensted, 1985; Yool *et al.*, 1998).

For surface-area determinations, each MB cation is usually assumed to lie flat on the basal surface of the clay, covering ~130 Å^2 (Hang and Brindley, 1970). The strength of the method to study surface areas lies in its application to solvated surfaces, in contrast to gas-phase, dry-surface probes, such as N_2 in the BET method. The MB-ion method has been most successful in measuring Na-saturated clays and, in industrial applications, the relative smectite contents of bentonite deposits (Brindley and Thompson, 1970; Lagaly, 1981).

Surface areas and CEC are frequently overestimated (Hähner *et al.*, 1996; Inel and Askin, 1996; Mishael *et al.*, 1999) by the MB-ion method, but underestimation of CEC was also reported (Taylor 1985). Typical explanations for overestimation are that MB adsorbs in multiple layers (Hang and Brindley, 1970) or that it does not lie flat on the mineral surface (De *et al.*, 1974; Shelden *et al.*, 1993; Hähner *et al.*, 1996; Bujdák and Komadel, 1997). In some cases, excess-adsorption levels were explained by the formation of molecular aggregates on outer clay surfaces (Mishael *et al.*, 1999). Shariatmadari *et al.* (1999) proposed that adsorption of organic cations in excess of CEC is related to neutral sorption sites. In general, self-aggregation of dyes has been suggested by spectroscopic

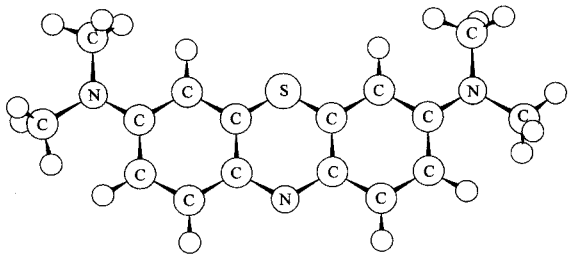

Figure 1. Schematic representation of methylene blue (the organic cation is shown without an anion).

investigations (Arbeloa *et al.*, 1997; Bergmann and O'Konski, 1963; Breen and Loughlin, 1994; Breen and Rock, 1994; Bujdak *et al.*, 1998; Garfinkel-Shweky and Yariv, 1997a, 1997b).

Some interlayer adsorption mechanisms were inferred from *d*(001) values determined by X-ray diffraction of clay-MB systems. Values for *d*(001) of 12.6–15.2 Å, depending on the mineral type, are thought to correspond to monolayers in which the molecular plane of MB lies parallel to the basal surface of the clay (Hang and Brindley, 1970; Yariv and Lurie, 1971). In view of results obtained for the aromatic dye acridine orange (Garfinkel-Shweky and Yariv, 1997a), parallel sorption of MB ions was proposed to involve π interactions in which oxygen atoms from the oxygen planes of the siloxane sheet of the clay donate lone-pair electrons to π antibonding orbitals of the organic cations.

A *d*(001) value of ~15.6 Å was postulated (Cenens and Schoonheydt, 1988; Hang and Brindley, 1970) to arise from parallel MB bilayers in hectorite and montmorillonite interlayers. Montmorillonite *d*(001) values observed at 17.2–17.7 Å (Bodenheimer and Heller, 1968; Hang and Brindley, 1970) were interpreted to involve MB molecules adsorbed at an angle close to 90° relative to the basal plane (Bujdák and Komadel, 1997). On mica, the molecular plane seems to adopt an angle of ~70° with respect to the basal plane (Hähner *et al.*, 1996), which is consistent with the charge on a mica layer being nearly four times that of smectite.

MB is an aromatic cation (Figure 1) which allows its rate of adsorption and adsorption equilibria to be probed by optical absorption spectroscopy (Schoonheydt and Heughebaert, 1992; Gessner *et al.*, 1994; Bujdák and Komadel, 1997). There is some disagreement about the meaning of the ultraviolet (uv)-visible (vis) spectroscopy data. Gessner *et al.* (1994) suggested that only MB monomers exist in the interlayer of montmorillonite. However, others (Cenens and Schoonheydt, 1988, 1990; Schoonheydt and Heughebaert, 1992) have argued that dimers are very common. In addition, Bujdák and Komadel (1997) proposed that higher-order agglomerates (perhaps adsorbed on edges) are also possible, depending primarily on the local surface-charge density.

The exact mechanisms of how MB adsorbs to clay minerals are largely unknown and are expected to be rather complex (Bodenheimer and Heller, 1968). For this reason we have used molecular-dynamics simulations to explore what structural arrangements and interactions of MB ions with clay mineral surfaces are energetically stable. Specifically, MB adsorption on a model beidellite crystal at various surface loadings, and the interactions of MB with a model mica surface were investigated in detail.

COMPUTATIONAL PROCEDURES

The clay-mineral force field of Teppen *et al.* (1997) was used in all calculations together with the MSI/Discover molecular modeling software suite, version 4.0.0 (MSI, 1996). The force-field parameters chosen were developed specifically for dioctahedral clays (Teppen *et al.*, 1997) and enable full dynamics simulations where both the mineral surface and the adsorbed phase are dynamic. In the recent past, simulations of this kind have successfully reproduced various clay-mineral crystal structures, and simulations of the swelling of Na-saturated and Ca-saturated beidellite clays at many different H_2O contents yielded *d*(001) values within experimentally observed ranges (Teppen *et al.*, 1997). In a study of the sorption of trichloroethene (Teppen *et al.*, 1998) the clay-mineral force-field parameters could be successfully used with parameters established for organic molecules.

Parameters for organics and H_2O molecules were taken from the CFF91 force-field dataset of MSI (1996). The simulations reported here used the InsightII/Discover molecular modeling suite (MSI, 1996), which employs the Parrinello-Rahman method to control pressure, and direct velocity scaling to control temperature. All calculations employed three-dimensionally periodic boundary conditions, and no space group symmetry was imposed other than *P*1. The molecular-dynamics time step was 0.5 fs and the simulations were typically executed for 100–300 ps, as described below. The conditions applied during dynamics were either constant pressure and temperature (NPT), or constant volume and temperature (NVT), as described in each case below.

We used Ewald-inspired lattice sums of Karasawa and Goddard (1989), as implemented in the Discover code, for calculating both the Coulombic and dispersive contributions to the energies and forces. In this scheme, the Ewald parameter is automatically chosen (based on unit-cell dimensions) and an energy-accuracy parameter is specified (at 0.025 kcal mol^{-1}). These two values were used to calculate the real-space and reciprocal-space cutoffs necessary to achieve the given accuracy (Karasawa and Goddard, 1989). Short-range van der Waals repulsion energies were computed

in the all-image convention, again using the accuracy parameter to determine unit-cell-dependent cutoff radii. Tests of this overall method show that non-bonded energies are accurate to within 0.05% of their asymptotic values. The method was used for all simulations reported here.

Several series of simulations were executed for this study. In the first series, an expanded pyrophyllite (Lee and Guggenheim, 1981) was produced by taking 4 × *a*, 2 × *b*, and 1 × *c* unit cells to produce an $Al_{32}Si_{64}O_{160}(OH)_{32}$ supercell of neutral, idealized, 2:1 clay. Six Si ions in the tetrahedral sheet of the neutral supercell were then isomorphically substituted with Al to simulate an idealized beidellite with a CEC of 105 meq/100 g. Subsequently, 2, 4, or 6 monovalent MB cations were adsorbed on the dry (without H_2O) interlayer with 2, 1, or 0 Ca^{2+} ions, respectively, corresponding to surface loading rates of ~35, ~70, and ~105 meq of MB/100 g of clay, respectively. Henceforth, the basic supercells obtained in this way are referred to as beid421-2MB-dry, beid421-4MB-dry, and beid421-6MB-dry, respectively.

Limited evidence exists (Gessner *et al.*, 1994; Bujdak and Komadel, 1997) that MB can protonate to form a dication after adsorption on mineral surfaces. The adsorption properties of the dication probably differ significantly from those of the monovalent ion. Because of the length of the calculations, the current paper deals exclusively with the latter.

In a second series of calculations, H_2O was added to the beidellite supercells described above. In the case of beid421-2MB-dry, the interlayer was expanded to 35 Å, to add 106 H_2O molecules. This particular H_2O content, ~33 wt. % (*i.e.*, 0.33 g of water/g of clay), was selected to complete a bilayer of pure H_2O; that is, the amount of H_2O is sufficient to form a monolayer on each mineral surface without including the area of the MB ions. These models are referred to as beid421-2MB-106w.

For beid421-4MB-dry, 42 H_2O molecules were added, yielding a supercell henceforth referred to as beid421-4MB-42w. This corresponds to a H_2O content of 0.13 g/g; selected so that the total area of the combined adsorbates (42 H_2O plus 4 MB) is approximately equivalent to complete bilayer coverage of the beidellite basal planes. In a computer experiment testing the dependence of the *d* value on H_2O content, the number of H_2O molecules in beid421-4MB-42w was reduced in several steps, from 0.13 g/g to 0.10, 0.084, 0.071, and 0.062 g/g. The loadings yield the supercells beid421-4MB-33w, beid421-4MB-27w, beid421-4MB-23w, and beid421-4MB-20w. These specific H_2O contents resulted from eliminating individual H_2O molecules whose motion during dynamics led to positions between the H_2O bilayers.

In a third series of calculations, the crystal structure of muscovite (Comodi and Zanazzi, 1995) was used to construct an idealized and hypothetical mica structure by replacing up to six potassium ions by MB. The *c* axis of each supercell was expanded to ~80 Å to create a simulated external mica surface on which 1–6 MB ions were adsorbed, and these models were investigated in different dynamics simulations. This 80-Å separation represents a region where the phenomena occurring on one basal plane are not affected by phenomena occurring on others. To maintain the enlarged interlayer, the conditions of all simulations were NVT. The mica systems defined above are referred to as mica321-xMB-dry, where x = 1–6. When the "soak" option of the MSI InsightII/Discover software (MSI, 1996) was used to hydrate the dry mica surface, the default operation resulted in the addition of 147 H_2O molecules, yielding mica321-xMB-147w.

In a fourth series of calculations, the pyrophyllite supercell described above was modified to produce an idealized montmorillonite by replacing six Al ions in the octahedral sheet by Mg. Dynamics simulations were performed with potential parameters for Mg that are currently being refined. These preliminary simulations of a model montmorillonite were performed for systems with 2, 4, and 6 MB ions in the absence of H_2O. These supercells are referred to as mont421-2MB-dry, mont421-4MB-dry, and mont421-6MB-dry, respectively.

In support of future work, in Appendices 1 and 2 the Cartesian atomic coordinates are listed, which were obtained by dynamics simulations of two representative systems, beid421-2MB-dry and beid421-2MB-106w.

RESULTS AND DISCUSSION

Adsorption at beidellite model surfaces

The dynamics simulations of beid421-2MB-dry (corresponding to ~35 meq of MB/100 g of beidellite), beid421-4MB-dry (~70 meq/100 g), and beid421-6MB-dry (~105 meq/100 g) yielded equilibrated systems with *d*(001) values of 12.3, 12.9, and 15.7 Å, respectively. X-ray studies of MB adsorption on montmorillonite *in vacuo* (Hang and Brindley, 1970) yielded *d*(001) values of 12.6, 14.8, and 15.6 Å, respectively, for loads of ~20–60, 40–90, and 60–120 meq MB/100 g montmorillonite.

The simulated structure of beid421-2MB-dry is given in Figure 2. It shows that, at relatively low loads (~35 meq/100 g) and in the absence of water, MB can form a single layer parallel to the (001) plane. In the presence of water (Figure 2), simulations of beid421-2MB-106w did not yield such a layer in 150 ps, but the MB ions assembled preferentially in the solvation sphere. This behavior is the same as that found for trichloroethene (Teppen *et al.*, 1998), which adsorbs flat on dry-mineral surfaces, but resides mainly in the solvation sphere in the presence of H_2O. Compared to

https://doi.org/10.1346/CCMN.2000.0480608 Published online by Cambridge University Press

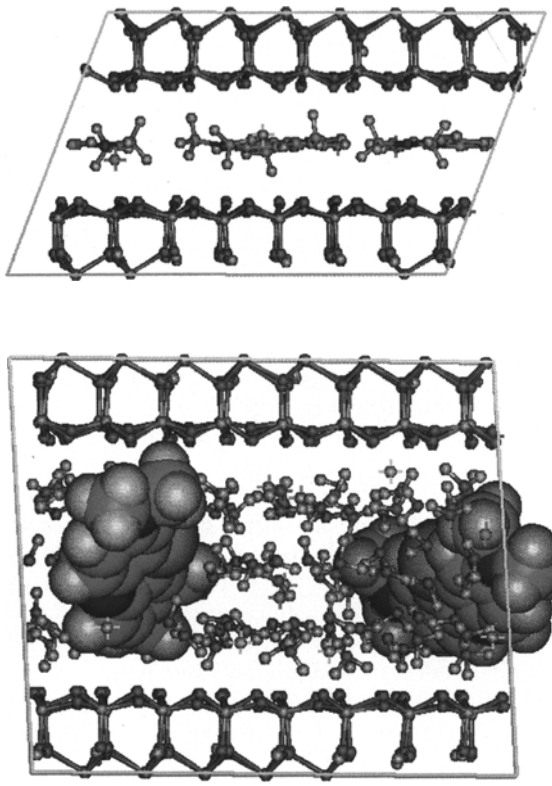

Figure 2. Adsorption of methylene blue on model beidellite in the absence (top) and presence (bottom) of H_2O. The top figure shows NPT molecular-dynamics results for 2 MB ions adsorbed in the supercell, beid421-2MB-dry, as described in the text. The MB loading is ~35 meq/100 g. The H_2O content in the cell shown below (beid421-2MB-106w; see text) is 0.33 g/g, which corresponds to a bilayer of pure H_2O for the system and a triple layer when MB is included.

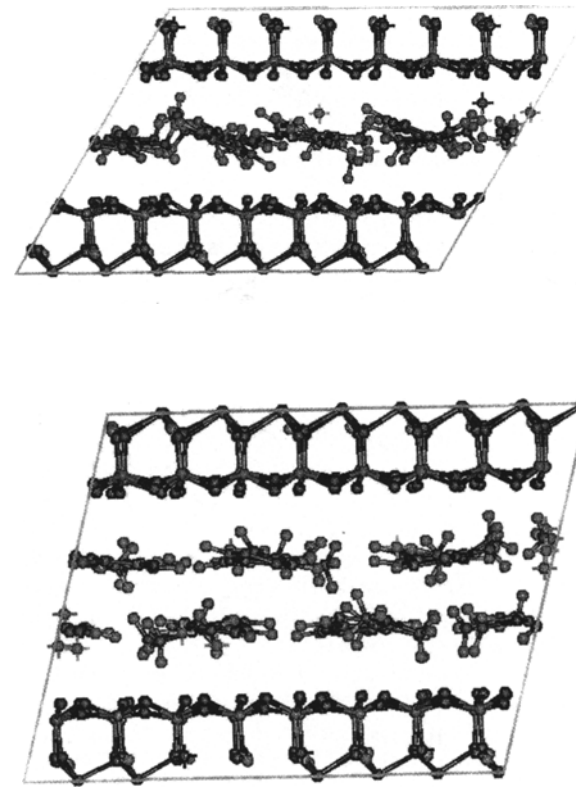

Figure 3. NPT molecular-dynamics results of MB adsorption on dry model beidellite at MB loadings of ~70 meq/100 g clay (top, supercell beid421-4MB-dry) and ~105 meq/100 g (bottom, supercell beid421-6MB-dry).

beid421-2MB-dry, the $d(001)$ value of beid421-2MB-106w increased from 12.6 to 17.7 Å. Note that the H_2O molecules in beid421-2MB-106w are arranged in three distinct parallel layers (Figure 2), which formed from an initially random arrangement.

At ~70 meq/100 g, the structure resulting from the simulations of beid421-4MB-dry consists of a molecular stack (Figure 3) in which the ions are slightly nonparallel to the basal plane, and their projections on the latter overlap. The angle of inclination is 15–20°. At ~105 meq/100 g, the simulations of beid421-6MB-dry yielded a bilayer parallel to the basal planes (Figure 3).

Additional simulations show that all dry configurations are generally perturbed by the addition of H_2O, resulting either in complete solvation of ions, if the H_2O content is sufficiently high, or in layered ion-H_2O structures, involving MB and H_2O, such as the one shown in Figure 4 for beid421-4MB-42w. The latter presents an interesting phenomenon. When beid421-4MB-42w was subjected to NPT simulations, starting with the random configuration shown in Figure 4, within ~10–20 ps the organized MB-H_2O bilayer of Figure 4 appeared. In continued simulations, which extended through 100 ps, the layer remained stable and essentially unchanged.

To test to what extent the formation of the ion-H_2O bilayer depended on the mode of simulation, the starting configuration of beid421-4MB-42w (Figure 4) was first equilibrated in 100 ps of NVT simulations, and then subjected to 200 ps of NPT simulations. In this series, an identical MB-H_2O bilayer was formed again and remained stable throughout the entire cycle.

To determine the importance of the starting configuration on the emergence of the mixed ion-H_2O bilayer, the random arrangement of the MB ions in the starting configuration of beid421-4MB-42w (Figure 4) was replaced by a well-ordered parallel stack, where the MB ions were arranged perpendicular to the mineral (001) plane. NPT simulations of this supercell then yielded, within ~10–20 ps, a local-energy minimum in which the MB ions were locked in a parallel stack nearly perpendicular to the (001) plane at ~100 kcal/mol above the ion-H_2O bilayer described above. Because additional dynamics simulations (200 ps) failed

https://doi.org/10.1346/CCMN.2000.0480608 Published online by Cambridge University Press

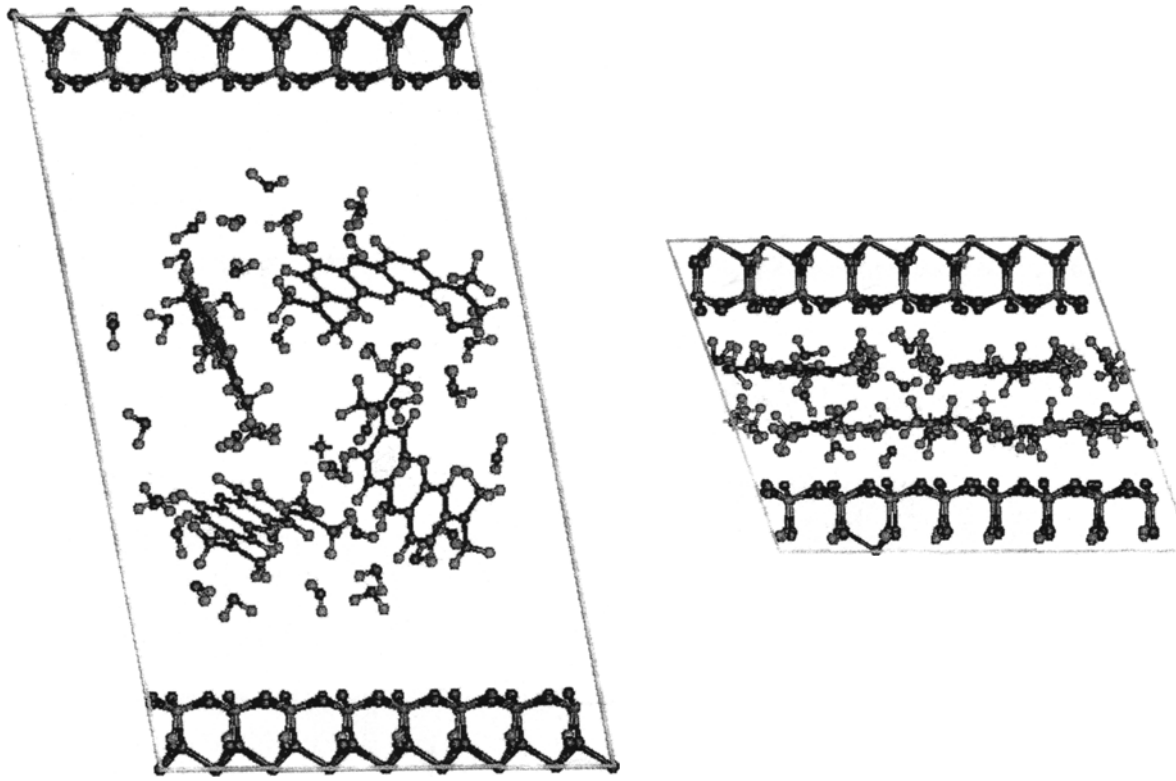

Figure 4. NPT molecular-dynamics results of MB adsorption (~70 meq/100 g clay) on model beidellite with 0.13 g H_2O/g clay, representing the supercell, beid421-4MB-42w, as described in the text. At the selected MB loading, the combined areas of the MB ions and H_2O approximately correspond to an ion-H_2O double layer. The starting cell structure is given on the left; the final structure, on the right.

to remove the system from this high-energy local minimum, the temperature was simulated at 1000 K, and the system then cooled to 300 K at a rate of 100 K per 10 ps by using simulated annealing. This procedure yielded essentially the same ion-H_2O bilayer as shown in Figure 4.

The d(001) values found for dry parallel, or approximately parallel, monolayers of MB range from 12.3 to 12.9 Å. Thus, the same structure is assigned to the system found by Hang and Brindley (1970) *in vacuo* at 12.6 Å. Similarly, the value of 15.6 Å observed by Hang and Brindley for high loads is assigned to a parallel bilayer of MB that may form in the interlayer in the absence of H_2O (calculated value 15.7 Å).

We did not find a dry supercell with the d(001) value of 14.8 Å as reported by Hang and Brindley (1970) in the region of 40–90 meq/100 g. However, the series of simulations involving beid421-4MB-33w, beid421-4MB-27w, beid421-4MB-23w, and beid421-4MB-20w yielded d(001) values of 15.4, 15.1, 15.0, and 14.4 Å, respectively. Thus, varying the H_2O content at constant MB loadings yields a range of d(001) values which include those observed by Hang and Brindley (1970).

The structures of the equilibrated supercells of the series beid421-4MB-(42w; . . . 33w; . . . 27w; . . . 20w) are also interesting because they show how changes in H_2O content can affect ion arrangement. In this case, specifically, reducing the amount of H_2O produces a transition from a relatively ordered ion arrangement (Figure 4) to a disordered configuration (Figure 5).

To determine the effects of charge location (octahedral *vs.* tetrahedral) on d(001) values, calculations were performed for supercells mont421-2MB-dry, mont421-4MB-dry, and mont421-6MB-dry. The resulting d(001) values are 12.3, 12.8, and 15.8 Å, respectively. They differ insignificantly from the 12.3, 12.9, and 15.7 Å found for the corresponding beidellite series. This indicates that d(001) values are not significantly affected by charge location.

Adsorption on mica surfaces

Recently, the structure and orientation of MB on muscovite mica were investigated with X-ray photoelectron spectroscopy (Hähner *et al.*, 1996). In these experiments, a regular stack of MB ions was found where individual molecules are tilted with their largest plane at 65–70° with respect to the mica (001) plane.

https://doi.org/10.1346/CCMN.2000.0480608 Published online by Cambridge University Press

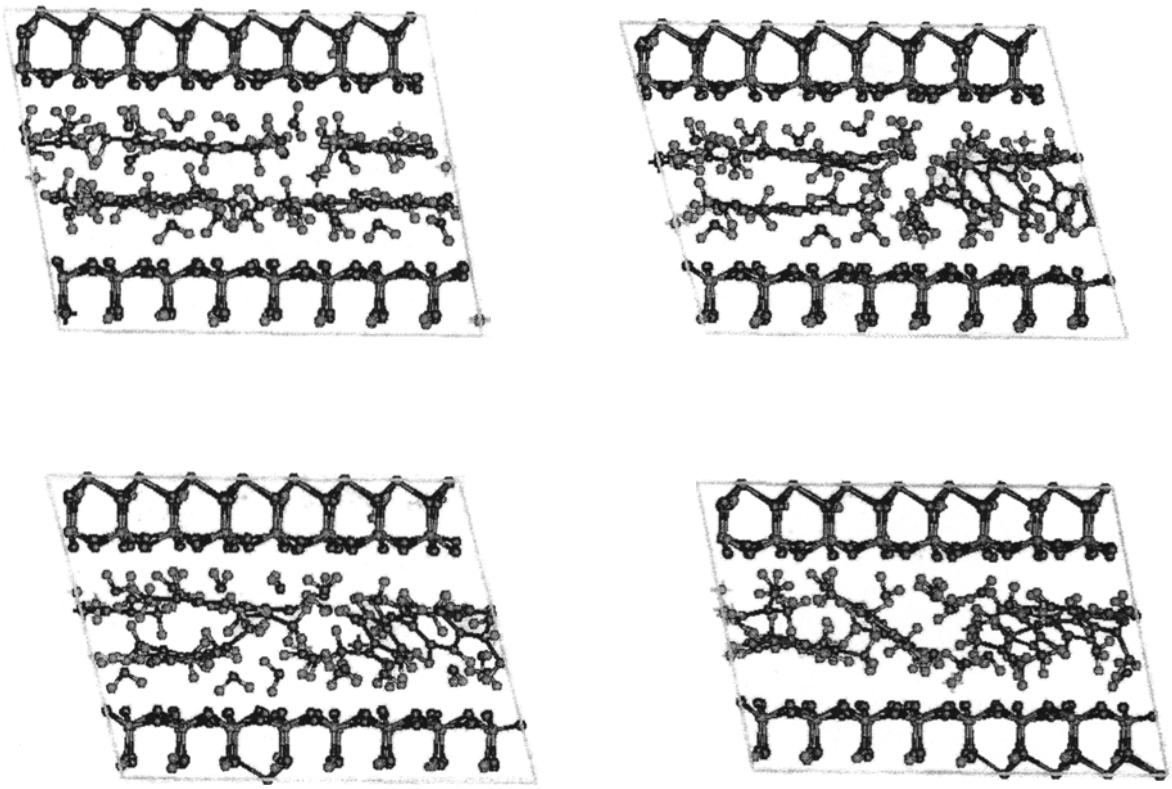

Figure 5. NPT molecular dynamics results of MB adsorption (~70 meq/100 g clay) on model beidellite, illustrating the structural effects of reducing the H_2O content from 0.10 g/g (top left) to 0.084 g/g (top right), 0.071 g/g (bottom left), and 0.062 g/g (bottom right). For additional details see the text.

Dynamics simulations with one to six MB ions on the dry mica surface described above yielded a variety of orientations, none of which agreed with experiment. At low loads, where one and two MB ions were adsorbed, the molecules oriented flat on the (001) plane. At increasing loads, some of the molecules assumed a tilted orientation relative to the (001) plane, forming a mixture of flat, tilted, and random piles. The equilibrated structures for one and six MB ions are shown in Figure 6.

These results are independent of the starting conditions. Even for dynamics simulations initiated with the structure given by Hähner *et al.* (1996), irregular clusters formed spontaneously. In contrast, when the mica-MB supercell was saturated with H_2O, as described above, configurations resulted from NVT dynamics of mica321-xMB-147w, which are similar to those proposed by Hähner *et al.* (1996), albeit not as strictly ordered and not ordered in exactly the same way. From the initially random configuration (Figure 6), some of the ions in mica321-4MB-147w oriented at a high angle to the (001) plane, forming loosely associated configurations. As shown below, the degree of disorder did not change through 350 ps of simulation and the ions display a degree of mobility that is not compatible with regular crystal order.

Estimates of projected areas and the formation of aggregates

The projected molecular area of MB was given as 130 Å^2 (Hang and Brindley, 1970). The value is based on the assumption that the molecule is a rectangle of dimensions 17.0 Å × 7.6 Å.

→

Figure 6. NVT molecular-dynamics results of MB adsorption on dry-model muscovite surfaces with 1 (top left) and 6 (top right) MB ions adsorbed on the surface of the supercell, mica321-nMB-dry, as described in the text. Where 4 MB ions are adsorbed and the system is in excess of H_2O molecules (supercell, mica321-4MB-147w), the final cell structure (bottom right) is obtained from the initial structure shown on the bottom, left. For reasons of clarity, MB ions are rendered in the space-filling (van der Waals) display mode, whereas H_2O molecules and minerals surfaces are rendered in the ball-and-stick display mode.

https://doi.org/10.1346/CCMN.2000.0480608 Published online by Cambridge University Press

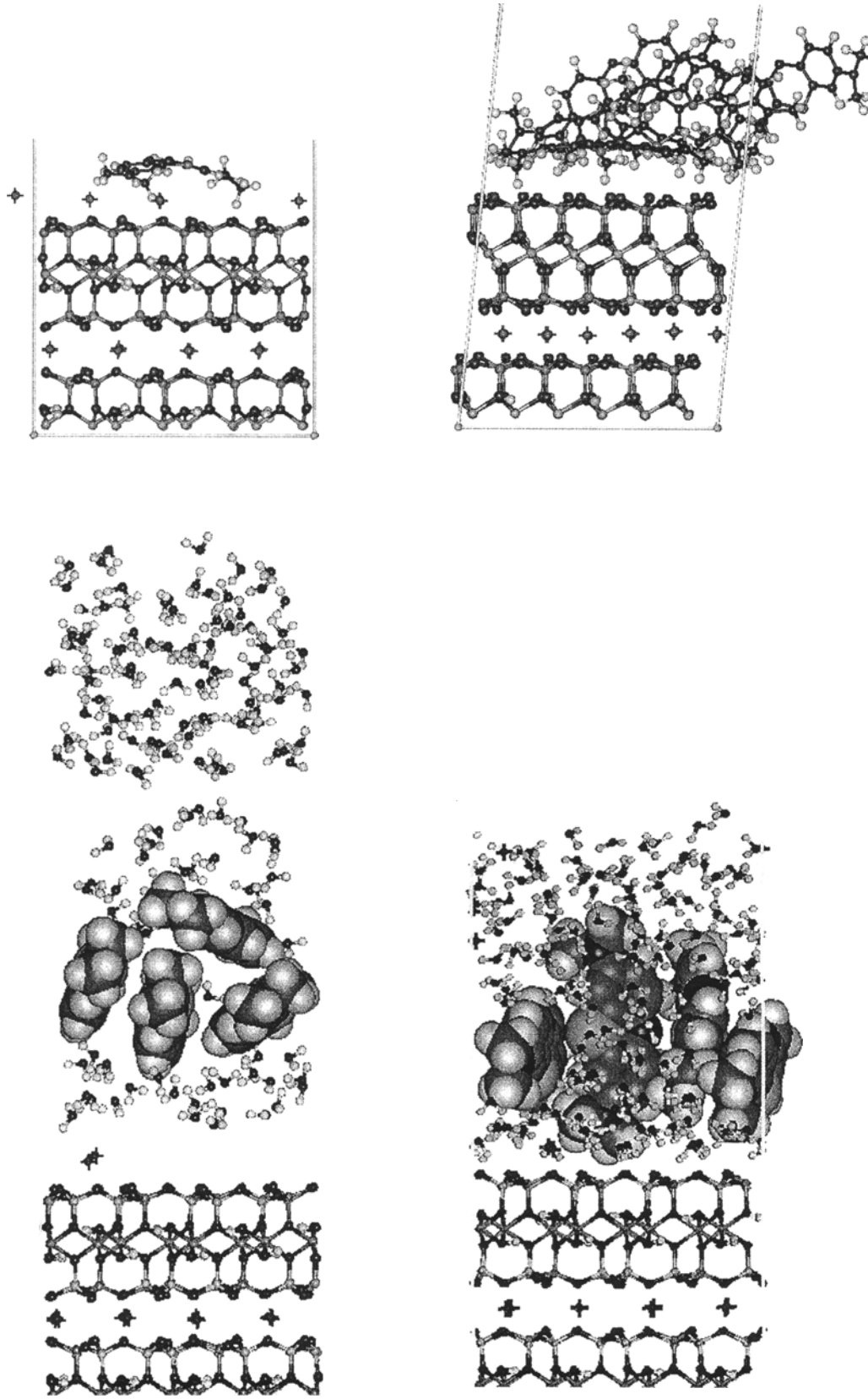

https://doi.org/10.1346/CCMN.2000.0480608 Published online by Cambridge University Press

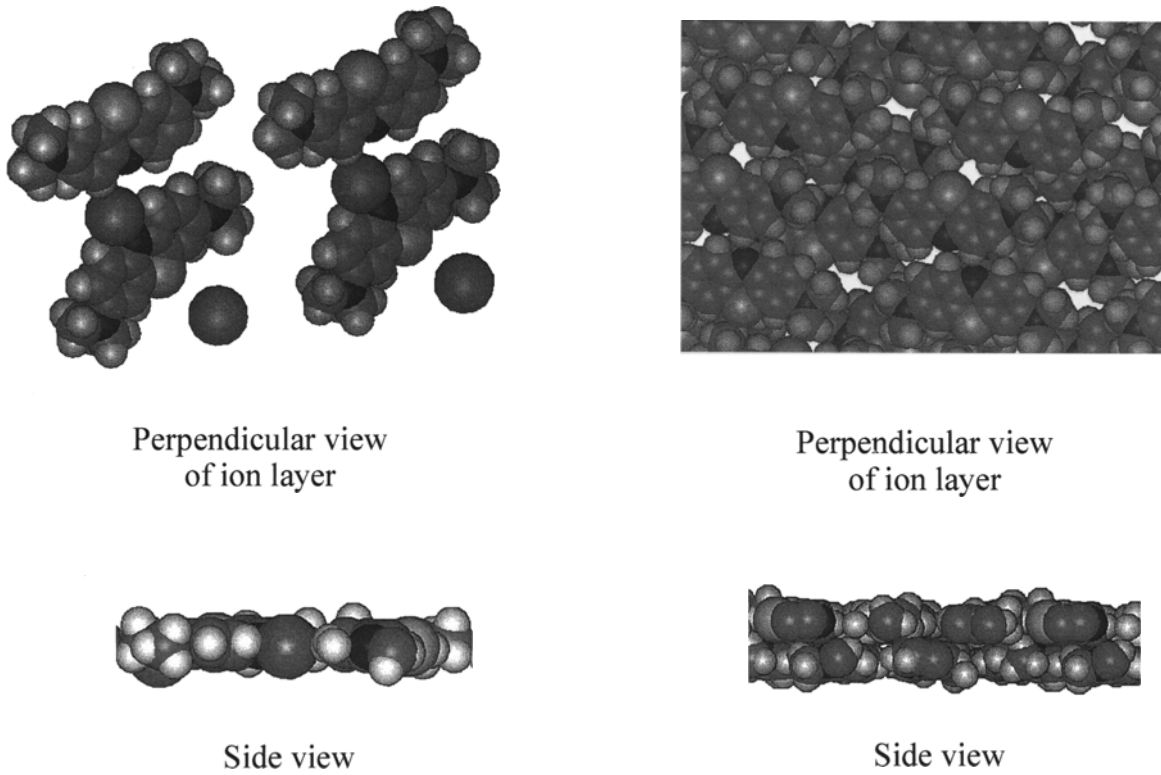

Figure 7. Associations of MB ions in beid421-2mb-dry (left graphs) and beid421-6mb-dry (right graphs). Where two MB ions are adsorbed (~35 meq/100 g), they form a single layer parallel to the basal plane (bottom, left). They do not form dimers but are separated by calcium ions (top, left). With 6 MB ions adsorbed (~105 meq/100 g), attractive intermolecular interactions between MB ions are the rule (top, right) and a double layer is formed parallel to the basal plane (bottom, right). Only the adsorbate layers are shown in this Figure.

When the outline of an MB ion was examined closely in the solid-render display mode of the MSI/Discover software, a molecular area of ~102 Å^2 was obtained. This is the minimum area covered by an isolated ion adsorbed on a clay surface in a single layer, flat and parallel to the basal plane. However, the actual area occupied by an ion parallel to the (001) plane should be greater than 102 Å^2, because the shape of the molecule does not allow for contiguous surface coverage. Thus, our estimate for an isolated molecule compares favorably, though not exactly, with the estimate of 130 Å^2 proposed by Hang and Brindley (1970) for the effective area of MB in the context of adsorption. In addition, uncertainties in van der Waals radii have an effect on calculated area.

In any case, the results described above show that the projected areas of single MB ions on clay-mineral surfaces are rather variable, especially in the presence of H_2O. When an area of 102 Å^2 is inclined at 18° with respect to the basal plane, a projected area of 97 Å^2 results. Similarly, the projected area per ion in a parallel double layer will differ from that in a monolayer. However, different estimates of surface coverage result when the projected areas overlap. For example, for a stack inclined at 18°, an effective area of 87 Å^2 (rather than 97 Å^2) was found. Thus, MB adsorption on clays can involve surface areas smaller than the molecular area of an isolated ion. This is in agreement with prior observations (Hähner *et al.*, 1996) that clay-surface areas can be overestimated.

The formation of aggregates of MB ions on clays was discussed by Cenens and Schoonheydt (1988, 1990), Schoonheydt and Heughebaert (1992), Gessner *et al.* (1994), and Bujdák and Komadel (1997). The dynamics simulations can be used to illustrate some of the intermolecular interactions that MB ions exhibit (Figures 7 and 8).

At low loads (35 meq/100 g) on beidellite, the simulated MB ions do not associate. Instead (Figure 7), pairs of adsorbates are found which were separated by Ca^{2+}. In contrast, for higher loading rates, for example in the simulations with six MB ions (Figure 7), numerous intermolecular contacts were formed within the standard nonbonded radii. The same result was obtained for mica (Figure 8), where the adsorbed ions displayed particularly varied interactions. For the system with three MB ions (Figure 8), interactions were directed not only from one side of an ion to another,

https://doi.org/10.1346/CCMN.2000.0480608 Published online by Cambridge University Press

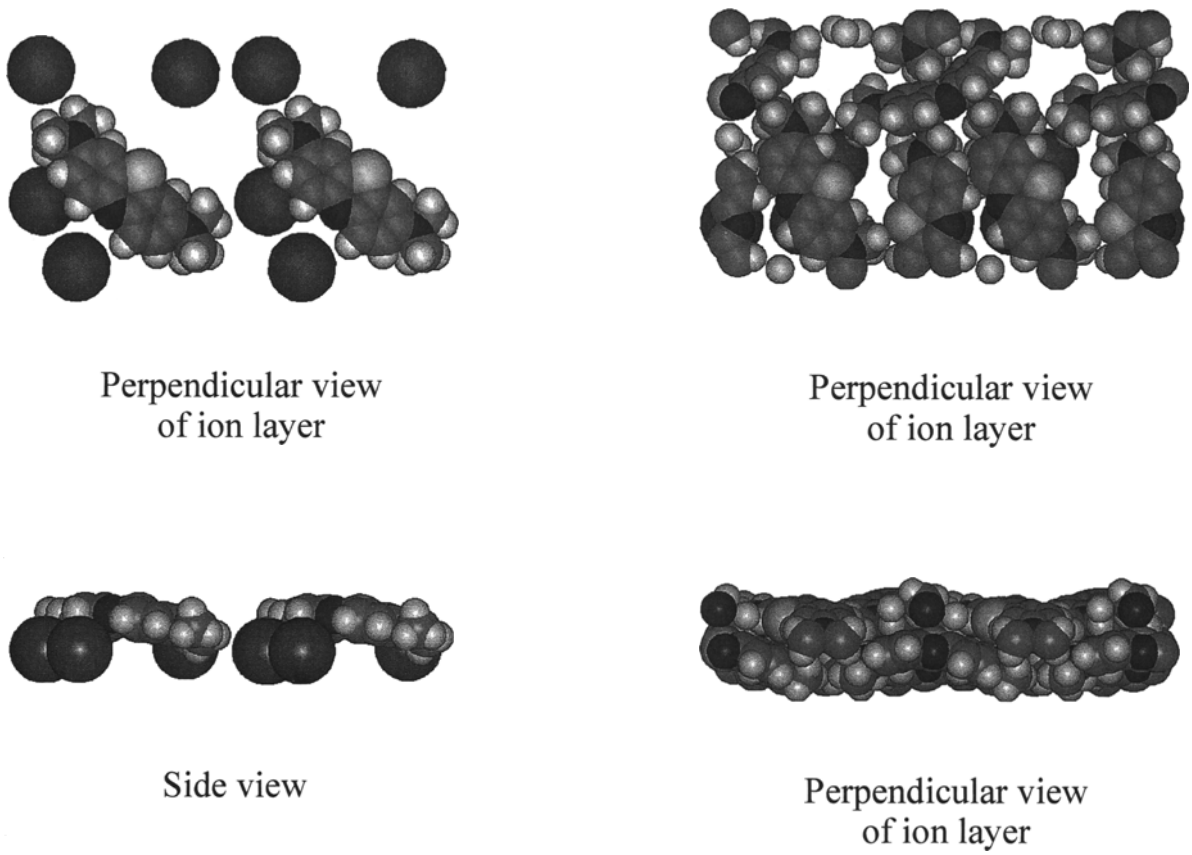

Figure 8. Associations of MB ions on dry muscovite surfaces, representing the systems, mica321-nMB-dry, as described in the text. Where 1 MB ion is adsorbed on the model surface, (mica321-1MB-dry, left, top and bottom), it assumes a position parallel to the basal plane. Where 3 MB ions are adsorbed (mica321-3MB-dry, top, right) they are seen to aggregate sidewise, and by attaching the end of one onto the plane of another. Dynamics simulations of a system with 5 MB ions (mica321-5MB-dry) yielded a characteristically wavy double layer (bottom, right). Only the adsorbate layers are presented in this Figure. This model is observed seen along a line perpendicular (top) and parallel (bottom) to the basal plane.

but also from one end of one ion to the center of another. In simulations with five MB ions, a closely packed wavy double layer resulted (Figure 8). Thus, it seems that aggregation is spontaneous and maintained by a variety of non-bonded interactions.

Analysis of the dynamics

Additional information on MB adsorption is obtained from an analysis of ion motion during MD simulation. Various properties can be used in the analysis. Those analyzed in this study will be defined in the following paragraphs. Following the evolution of such variables during dynamics simulations allows the characterization of the motion of the ions in the interlayer region. Representative results are given in Figures 9–12.

The z-distance is defined as the perpendicular distance from the (001) plane to a representative atom in a given MB ion. Following this distance during dynamics illustrates how the ion moves from an arbitrary starting position toward the clay surface until an equilibrium position is reached. Analyses of the dynamics files show that the MB ions move quickly, within a few ps after the start of the simulations, to stable and relatively constant z-distances, where fluctuations are only a few tenths of an Å. In moving to the final positions, the adsorbed ions display a clear tendency for turning in such a way that the methyl groups point towards the mineral surface.

The long axis is defined as the line intersecting the two $N(CH_3)_2$-nitrogen atoms in the MB molecule (Figure 1). The short axis is defined as the line intersecting the N and S atoms of the central ring (Figure 1). The orientations of these axes are measured by the angles relative to the normal to the (001) plane. Spin is defined as the orientation of the long axis in the (001) plane. It is measured by the angle between the *a* axis and the projection of the long axis on the (001) plane.

Some representative axis orientations and spins are shown in Figure 9 for beid421-2MB-dry and beid421-2MB-106w, illustrating a striking difference between the conditions on dry and hydrated surfaces. Figure 9

https://doi.org/10.1346/CCMN.2000.0480608 Published online by Cambridge University Press

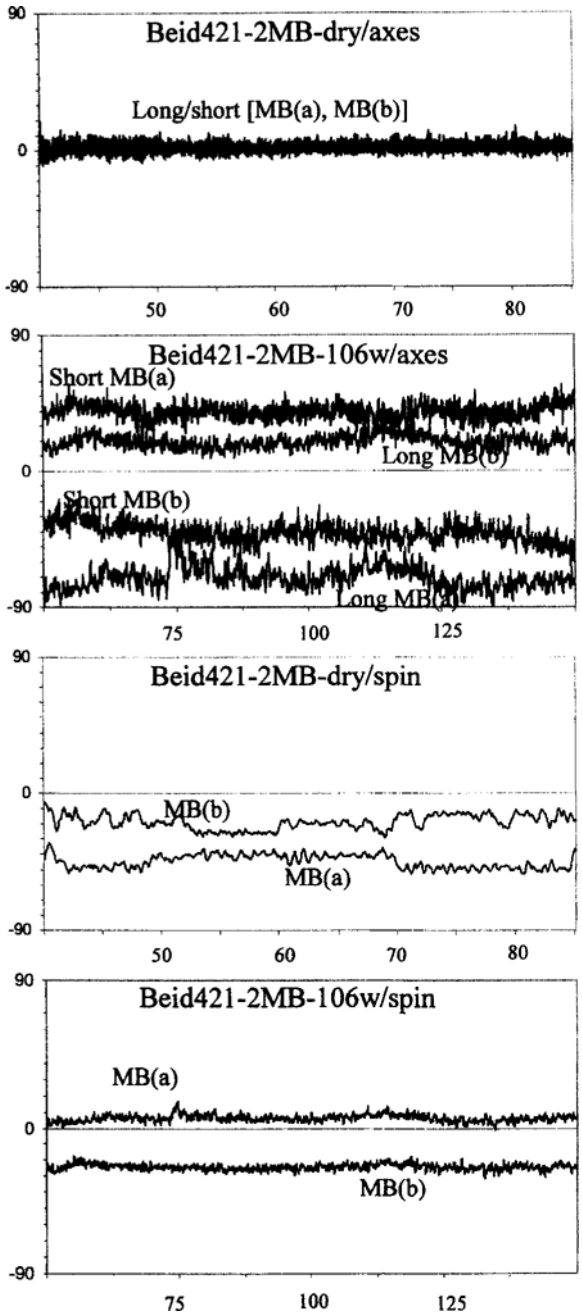

Figure 9. Comparison of the dynamics traces of beid421-2MB-dry and beid421-2MB-106w. The graphs show, for the two MB ions, MB(a) and MB(b), the angle with the (001) plane for the long and short axes (top two graphs), and the spin angles (bottom two graphs), as defined in the text. Angles (°) are plotted on the ordinate *versus* the time steps (ps) of the dynamics simulations, on the abscissa. In the case of beid421-2MB-dry, values for the last 45 ps of a total of 85 ps of simulations are shown. For beid421-2MB-106w, values for the last 100 ps of simulations of a total of 150 ps are shown.

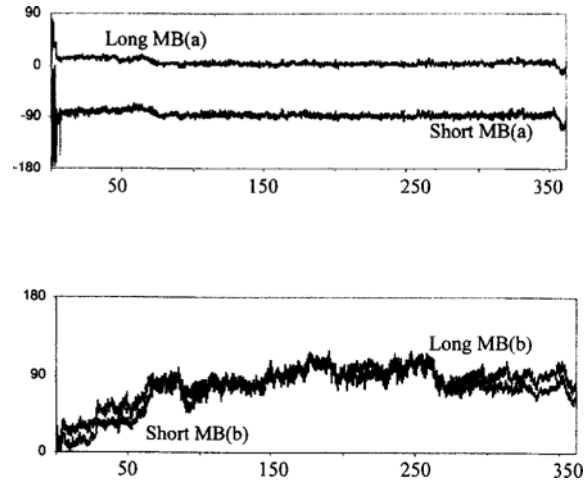

Figure 10. Dynamics traces for mica321-4MB-147w, showing the angle with the (001) plane for the long and short axes of two representative MB ions. Axes as defined in Figure 9.

shows that fluctuations in axis orientations are relatively small for adsorbates on dry surfaces, and high for hydrated systems. Interestingly, opposite trends are found for spins, where fluctuations are relatively high for dry systems, and low for wet. For beid421-2MB-dry, the orientations of each axis are similar, and the four curves merged into one (Figure 9).

Figure 10 of mica321-4MB-147w shows that, even under the same conditions and within the same system, some MB ions are nearly fixed in space, whereas others continue for long periods to migrate in the solvation phase. Figure 10 is a result of simulations to 360 ps. Figures 9 and 10 also illustrate that ions in the presence of H_2O may stabilize with different orientations, whereas those on dry surfaces all have a parallel orientation to the (001) plane.

Translational motion relative to the crystal (001) plane is illustrated in Figure 11, which shows projections of the S atoms in MB ions onto the (001) plane. It is seen from Figure 11 that ions adsorbed in the interlayer space are relatively immobilized compared to ions on open surfaces. The differences seen here for beid421-2mb-106w and mica321-4MB-147w are striking. These differences may reflect the increased steric interactions and electrostatic attractions, from adjacent 2:1 layers, compared to open surfaces.

In order to determine to what extent the translational motions of the various ions are correlated, the S to S non-bonded distances for the four MB ions of mica321-4MB-147w, MB(a) to MB(d), were determined and two representative graphs are plotted in Figure 12. Figure 12 shows that the motions of MB(b) and MB(c) are highly correlated, whereas other ions move independently.

https://doi.org/10.1346/CCMN.2000.0480608 Published online by Cambridge University Press

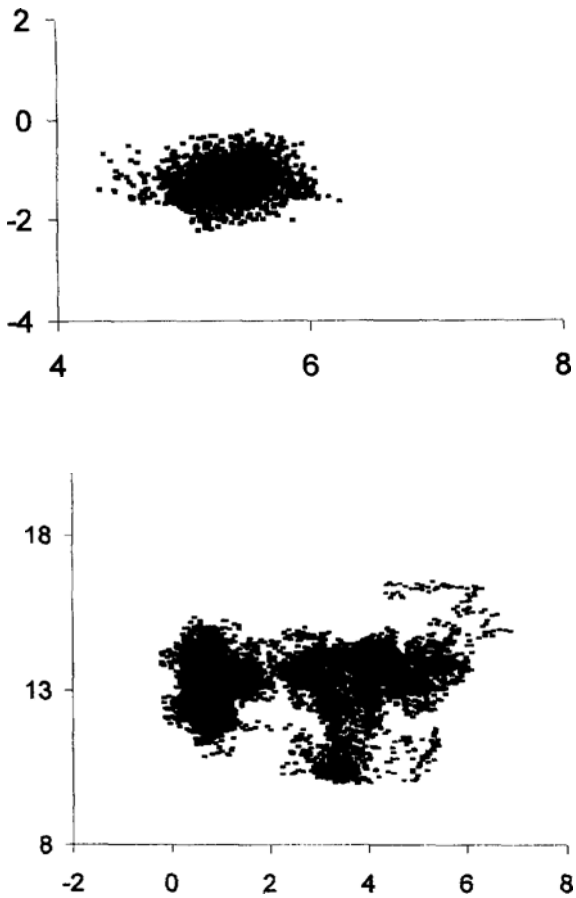

Figure 11. Projections of S-atom positions on the (001) plane of a representative MB ion in beid421-2mb-106w (top) and in mica321-4MB-147w (bottom). The values shown are distances (Å) from the unit-cell origin in a Cartesian x,y-plane, which coincides with the crystallographic axes in the (001) plane. The graphs are indicative of the translational motions, relative to the (001) plane, of the MB ions during the dynamics simulations described in the text.

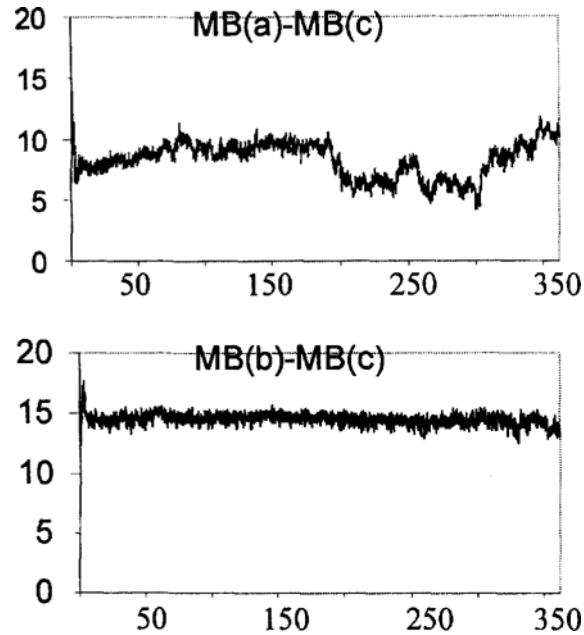

Figure 12. The evolution of intermolecular, non-bonded S to S distances (Å) between the sulfur atoms in two MB ions, MB(a)-MB(c) (top) and MB(b)-MB(c) (bottom), in mica321-4MB-147w, during dynamics simulations.

CONCLUSIONS

MB ions on clay-mineral surfaces can form a variety of aggregates. Specifically, MB-ion adsorption yields single and double layers parallel to the basal plane, with and without the inclusion of H_2O, and molecular stacks where the main plane of the adsorbate is tilted with respect to the (001) plane.

Our simulations of MB on dry mica surfaces were unable to produce regular stacks deduced from X-ray absorption spectroscopy (Hähner *et al.*, 1996). Rather, orientations are found where the MB ions are flat and tilted on the surface, and clustered in irregular ways. Compared with these results, more ordered molecular associations, with features similar to those proposed by Hähner *et al.* (1996), are obtained for hydrated mica surfaces. However, the model systems are not ordered as strictly and not exactly in the same way as the interpretation of the experimental data by Hähner *et al.* (1996). Furthermore, the solvated ions display a degree of mobility that is not compatible with rigorous crystal packing.

To rationalize the above discrepancy, imperfections of the force field applied are possible along with differences in the experimental and model conditions. Alternatively, the experimental structure of MB ions on mica surfaces by Hähner *et al.* (1996) may be understood as an average structure that is a superposition of local configurations with some variability.

The formation of molecular aggregates, at sufficient loadings, appears to produce clusters. Non-bonded interactions between ions can involve different mechanisms, for example attractions between the sides of two ions, or between the end of one and the molecular plane of another. Aggregation is also indicated by correlated translational motion.

The dynamics analyses represent a particularly attractive feature of the model calculations. They indicate that clear differences are found between the properties of MB ions on dry and hydrated surfaces, and between species adsorbed in the interlayer and on open surfaces.

For surface area determinations, the simulations confirm the general experience that the method must be used with great caution owing to the variety of orientations that MB ions can adopt on clay surfaces. Thus, the method should be more useful for relative area determinations, performed under identical condi-

https://doi.org/10.1346/CCMN.2000.0480608 Published online by Cambridge University Press

tions, than absolute ones. At the same time, the flexibility of the MB-ions in adopting various surface orientations is an advantage for CEC determinations over a wide range of surface-charge densities.

ACKNOWLEDGMENTS

The authors gratefully acknowledge support by USDA CSREES grant 99-3517-7782 and by the IBM Shared University Research Program. Special thanks are due C. Geren, Vice Chancellor for Research, University of Arkansas, and J. Coffin, IBM.

REFERENCES

Arbeloa, F.L., Arbeloa, T.L., and Arbeloa, I.L. (1997) Spectroscopy of rhodamine 6G adsorbed on sepiolite aqueous suspensions. *Journal of Colloid and Interface Science*, **187,** 105–112.

Bensted, J. (1985) Application of the methylene blue test to cement raw materials. *Journal of Chemical Technology and Biotechnology*, **35A,** 181–184.

Bergmann, K. and O'Konski, C.T. (1963) A spectroscopic study of methylene blue monomer, dimer, and complexes with montmorillonite. *Journal of Physical Chemistry*, **67,** 2169–2177.

Bodenheimer, W. and Heller, L. (1968) Sorption of methylene blue by montmorillonite saturated with different cations. *Israel Journal of Chemistry*, **6,** 307–314.

Breen, C. and Loughlin, H. (1994) The competitive adsorption of methylene blue on to Na-montmorillonite from binary solution with n-alkylytrimethylammonium surfactants. *Clay Minerals*, **29,** 775–783.

Breen, C. and Rock, B. (1994) The competitive adsorption of methylene blue on to montmorillonite from binary solution with thioflavin T, proflavine and acridine yellow. Steady-state and dynamic studies. *Clay Minerals*, **29,** 179–189.

Brindley, G.W. and Thompson, T.D. (1970) Methylene blue adsorption by montmorillonites. Determinations of surface areas and exchange capacities with different initial cation saturations. *Israel Journal of Chemistry*, **8,** 409–415.

Bujdák, J. and Komadel, P. (1997) Interaction of methylene blue with reduced charge montmorillonite. *Journal of Physical Chemistry B*, **101,** 9065–9068.

Bujdák, J., Janek, M., Madejova, J., and Komadel, P. (1998) Influence of the layer charge density of smectites on the interaction with methylene blue. *Journal of Chemical Society-Faraday Transactions*, **94,** 3487–3492.

Cenens, J. and Schoonheydt, R.A. (1988) Visible spectroscopy of methylene blue on hectorite, laponite B, and barasym in aqueous suspension. *Clays and Clay Minerals*, **36,** 214–224.

Cenens, J. and Schoonheydt, R.A. (1990) Quantitative absorption spectroscopy of cationic dyes on clays. In *Proceedings of the 9th International Clay Conference, Strasbourg 1989*, V.C. Farmer and Y. Tardy, eds., Science Géologiques Memoire 85, 15–23.

Chu, C.H. and Johnson, L.J. (1979) Cation exchange behavior of clays and synthetic aluminosilica gels. *Clays and Clay Minerals*, **27,** 87–90.

Comodi, P. and Zanazzi, P.F. (1995) High-pressure structural study of muscovite. *Physics and Chemistry of Minerals*, **22,** 170–177.

De, D.K., das Kanugo, J.L., Chakravarti, S.K. (1973) Studies on the adsorption of methylene blue on and from vermiculite and asbestos. *Journal of Indian Chemical Society*, **L,** 507–510.

De D.K., das Kanugo, J.L., Chakravarti, S.K. (1974) Adsorption of methylene blue, crystal violet and malachite green on bentonite, vermiculite, kaolinite, asbestos, and feldspar. *Indian Journal of Chemistry*, **12,** 1187–1189.

Fischer, D., Caseri, W.R., Hähner, G. (1998) Orientation and electronic structure of ion exchanged dye molecules on mica: An X-ray absorption study. *Journal of Colloid and Interface Science*, **198,** 337–346.

Garfinkel-Shweky, D. and Yariv, S. (1997a) Metachromasy in clay-dye systems: The adsorption of acridine orange by Na-saponite. *Clay Minerals*, **32,** 653–663.

Garfinkel-Shweky, D. and Yariv, S. (1997b) The determination of surface basicity of the oxygen planes of expanding clay minerals by acridine orange. *Journal of Colloid and Interface Science*, **188,** 168–175.

Gessner, F., Schmitt, C.C., and Neumann, M.G. (1994) Time-dependent spectroscopic study of the interaction of basic dyes with clays. 1. Methylene blue and neutral red on montmorillonite and hectorite. *Langmuir*, **10,** 3749–3753.

Hähner, G., Marti, A., Spencer, N.D., Caseri, W.R. (1996) Orientation and electronic structure of methylene blue on mica: A near edge X-ray absorption fine structure spectroscopic study. *Journal of Chemical Physics*, **104,** 7749–7757.

Hang, P.T. and Brindley, G.W. (1970) Methylene blue adsorption by clay minerals. Determination of surface areas and cation exchange capacities. *Clays and Clay Minerals*, **18,** 203–212.

Inel, O. and Askin, A. (1996) Adsorption of monovalent cationic dyes on some silicates. *Turkish Journal of Chemistry*, **20,** 276–282.

Karasawa, N. and Goddard, W.A., III (1989) Acceleration of convergence for lattice sums. *Journal of Physical Chemistry*, **93,** 7320–7327.

Lagaly, G. (1981) Characterization of clays by organic compounds. *Clay Minerals*, **16,** 1–21.

Lee, J.H. and Guggenheim, S. (1981) Single crystal X-ray refinement of pyrophyllite-1*Tc*. *American Mineralogist*, **66,** 350–357.

MSI (1996) *Insight II/Discover Users Guides, Version 4.0.0.* Molecular Simulations Inc., San Diego, California.

Mishael, Y.G., Rytwo, G., Nir, S., Crespin, M., Annabi-Bergaya, F., Van Damme H. (1999) Interactions of monovalent organic cations with pillared clays. *Journal of Colloid and Interface Science*, **209,** 123–128.

Neumann, M.G., Schmitt, C.C., and Gessner, F. (1996) Time-dependent spectrophotometric study of the interaction of basic dyes with clays. 2. Thionine on natural and synthetic montmorillonites and hectorites. *Journal of Colloid and Interface Science*, **177,** 495–501.

Rytwo, G., Nir, S., Margulies, L. (1996) A model for adsorption of divalent organic cations to montmorillonite. *Journal of Colloid and Interface Science*, **181,** 551–560.

Rytwo, G., Nir, S., Margulies, L., Casal, B., Merino, J., Ruiz-Hitzky, E. and Serratosa, J.M. (1998) Adsorption of monovalent organic cations on sepiolite: Experimental results and model calculations. *Clays and Clay Minerals*, **46,** 340–348.

Saehr, D., LeDred, R., and Hoffner, D. (1978) Contribution on a l'etude des Interactions Vermiculite-Colorants Cationiques. *Clay Minerals*, **13,** 411–425.

Schoonheydt, R.A. (1994) Organization and spectroscopy of dyes on submicron-sized crystalline solids. In *Microchemistry: Spectroscopy and Chemistry in Small Domains*, H. Mashuhara, ed., Elsevier Science, Amsterdam, 469–482.

Schoonheydt, R.A. and Heughebaert, L. (1992) Clay adsorbed dyes: Methylene blue on Laponite. *Clay Minerals*, **27,** 91–100.

Schramm, L.L., Yariv, S., Ghosh, D.K., and Hepler, L.G. (1997) Electrokinetic study of the adsorption of ethyl violet and crystal violet by montmorillonite clay particles. *Canadian Journal of Chemistry*, **75,** 1868–1877.

Shariatmadari, H., Mermut, A.R., and Benke, M.B. (1999) Sorption of selected cationic and neutral organic molecules on palygorskite and sepiolite *Clays and Clay Minerals*, **47,** 44–53.

Shelden, R.A., Caseri, W.R., and Suter, U.W. (1993) Ion exchange on muscovite mica with ultrahigh specific surface area. *Journal of Colloid and Interface Science*, **157,** 318–327.

Taylor, R.K. (1985) Cation exchange in clays and mudrocks by methylene blue. *Journal of Chemical Technology and Biotechnology*, **35A,** 195–207.

Teppen, B.J., Rasmussen, K., Bertsch, P.M., Miller, D.M., and Schäfer, L. (1997) Molecular dynamics modeling of clay minerals. 1. Gibbsite, kaolinite, pyrophyllilte, and beidellite. *Journal of Physical Chemistry B*, **101,** 1579–1587.

Teppen, B.J., Yu, C.H., Miller, D.M., and Schäfer, L. (1998) Molecular dynamics simulations of sorption of organic compounds at the clay mineral / aqueous solution interface. *Journal of Computational Chemistry*, **19,** 144–153.

Viseras, C. and Lopez-Galindo, A. (1999) Pharmaceutical applications of some Spanish clays (sepiolite, palygorskite, bentonite): Some preformulation studies. *Applied Clay Science*, **14,** 69–82.

Xeidakis, G.S. (1996a) Stabilization of swelling clays by $Mg(OH)_2$. Changes in clay properties after addition of Mg-hydroxide. *Engineering Geology*, **44,** 107–120.

Xeidakis, G.S. (1996b) Stabilization of swelling clays by $Mg(OH)_2$. Factors affecting hydroxy-Mg-interlayering in swelling clays. *Engineering Geology*, **44,** 93–106.

Yariv, S. and Lurie, D. (1971) Metachromasy in clay minerals. Part 1. Sorption of methylene blue by montmorillonite. *Israel Journal of Chemistry*, **9,** 537–552.

Yool, A.I.G., Lees, T.P., and Fried, A. (1998) Improvements to the methylene blue dye test for harmful clay in aggregates for concrete and mortar. *Cement and Concrete Research*, **28,** 1417–1428.

E-mail of corresponding author: schafer@protein.uark.edu

(Received 18 October 1999; accepted 3 July 2000; Ms. 387; A.E. Randall T. Cygan)

Appendix 1. Atomic Cartesian coordinates (Å) for model beid421-2MB-dry.[1]

Elem	X	Y	Z
Al	3.27706	1.58226	0.06639
Al	0.71384	6.08633	0.00426
Al	3.31243	7.60053	0.00657
Al	0.67058	3.09443	0.01476
Si	4.05244	0.12460	2.78054
Si	−2.53826	−6.29104	9.70105
Si	1.38100	4.52360	2.66318
Si	0.10707	−1.72521	9.58719
Si	4.17155	3.02613	2.69304
Si	−2.55699	−0.11221	9.64968
Al	1.56270	7.49667	2.85817
Al	−0.04247	−4.73896	9.49535
O	3.95325	0.10370	1.13421
O	−2.34460	−6.31464	11.34014
O	1.40403	4.57298	1.03009
O	0.22527	−1.75324	11.23499
O	4.25600	2.91877	1.02109
O	−2.63427	−0.09882	11.28164
O	1.70542	7.36908	1.04202
O	−0.14541	−4.60601	11.29764
O	1.55627	1.72393	0.94622
O	−0.02830	1.12963	11.43454
O	4.21541	6.19574	0.91792
O	−2.62877	−3.40993	11.43619
H	1.07074	0.91519	0.79432
H	0.39809	1.97324	11.63642
H	3.63802	5.39999	0.81157
H	−2.16696	−2.60993	11.65775
O	0.38139	3.46818	3.31509
O	1.28754	−0.81136	8.84880
O	3.07856	8.04421	3.44752
O	−1.57598	−5.27352	8.96726
O	3.96721	1.62116	3.44416
O	−2.32520	1.31413	8.87778
O	1.04978	5.88245	3.47313
O	0.34487	−3.15585	8.91623
O	2.97451	4.09746	3.00990
O	−1.32138	−1.13882	9.32299
O	0.32651	8.70387	3.05253
O	1.26099	−5.91519	9.17038
Al	3.37200	10.63854	0.05618
Al	0.82231	15.12472	0.146809
Al	3.46859	16.61208	0.11031
Al	0.76422	12.15411	0.08067
Si	4.06608	9.13235	2.68807
Si	−2.41262	2.77413	9.68335
Si	1.61098	13.59707	2.81467
Al	0.18088	7.31537	9.57985
Si	4.31528	12.05399	2.71767
Si	−2.56688	8.88996	9.73486
Si	1.78728	16.59047	2.84174
Si	0.05087	4.41811	9.71263
O	3.87756	9.09398	1.10017
O	−2.33338	2.76046	11.33188
O	1.50670	13.67205	1.14326
O	0.33734	7.31322	11.38694
O	4.36297	12.00396	1.11662
O	−2.59899	8.98226	11.37373
O	1.81526	16.53892	1.17325
O	−0.00544	4.46512	11.35962
O	1.69682	10.75014	0.91268
O	0.05773	10.12550	11.41904
O	4.39320	15.22975	0.99480
O	−2.53324	5.68239	11.49815
H	1.28644	9.88793	0.86031
H	0.53160	10.95074	11.46888
H	3.97068	14.37126	0.93371
H	−1.99744	6.49915	11.58869
O	0.53999	12.58033	3.52710
O	1.24481	8.61911	8.96741
O	3.00887	17.42551	3.52756
O	−1.30792	3.84643	8.97971
O	3.98427	10.57982	3.45601
O	−2.11504	10.29042	8.94203
O	1.56096	15.07929	3.51560
O	0.61321	5.70851	8.96112
O	3.15121	13.08371	3.13615
O	−1.52853	7.74209	9.37532
O	0.47676	17.43160	3.18654
O	1.25007	3.39643	9.45862
Al	8.46628	1.64024	−0.04373
Al	5.92150	6.09843	0.01246
Al	8.47455	7.65254	0.03551
Al	5.84395	3.12053	−0.02063
Si	9.24939	0.14191	2.59655
Si	2.80256	−6.24828	9.58250
Si	6.64878	4.55931	2.67667
Si	5.33454	−1.63499	9.58133
Si	9.36332	3.02061	2.62024
Si	2.57215	−0.05833	9.62137
Si	6.78131	7.49590	2.67500
Si	5.08761	−4.57029	9.54914
O	9.08715	0.14061	0.97225
O	2.77650	−6.20468	11.23164
O	6.57628	4.58382	1.05842
O	5.45983	−1.70361	11.24445
O	9.41448	2.94919	0.97703
O	2.51915	−0.00344	11.26950
O	6.85894	7.48327	1.05103
O	5.03203	−4.47203	11.19328
O	6.80866	1.70655	0.84915
O	5.14388	1.22572	11.44603
O	9.38895	6.22837	0.84978
O	2.51386	−3.32205	11.36463
H	6.34233	0.86842	0.66444
H	5.68083	2.00312	11.54980
H	8.97994	5.37488	0.69160
H	2.94603	−2.46847	11.29880
O	5.52624	3.63067	3.39508
O	6.53742	−0.82507	8.93104
O	8.14886	8.08371	3.44770
O	3.79344	−5.21479	8.79611
O	9.11609	1.60576	3.26226
O	2.78467	1.35114	8.87142
O	6.42673	6.04973	3.40365
O	5.31481	−3.09956	8.88723
O	8.10976	3.98797	2.97646
O	3.89344	−0.89177	9.33288
O	5.55762	8.47233	2.97160
O	6.34542	−5.60203	9.29710
Al	8.55395	10.68250	0.05342
Al	6.02687	15.13451	0.03419
Al	8.62383	16.67190	−0.01856
Al	5.96878	12.14816	0.07423
Si	9.22174	9.11912	2.71868
Si	2.73246	2.80164	9.67889
Si	6.72731	13.58580	2.73534
Si	5.37869	7.36217	9.74927
Si	9.49885	12.04116	2.80470
Si	2.69000	8.92324	9.64899
Si	6.96170	16.54029	2.67195
Si	5.20085	4.41615	9.69753
O	9.13307	9.14837	1.10513
O	2.88048	2.80616	11.29188
O	6.66705	13.61079	1.06024
O	5.48337	7.33128	11.35588
O	9.52381	11.92936	1.15866
O	2.62780	9.01515	11.28255
O	7.03417	16.38935	1.08109
O	5.16282	4.46628	11.36947
O	6.88035	10.74979	0.92249
O	5.28545	10.16631	11.46314
O	9.50085	15.29863	0.91856
O	2.58504	5.73429	11.48611
H	6.46643	9.95890	0.59792
H	5.75853	11.06991	11.56532
H	8.98028	14.45179	0.90615
H	3.03658	6.59611	11.60547
O	5.66932	12.58608	3.47757
O	6.57188	8.28431	9.05904
O	8.32393	17.22093	3.28129
O	3.85723	3.78125	9.02446
O	9.29364	10.50733	3.47808
O	3.15729	10.30350	8.84860
O	6.81842	15.03320	3.43786
O	5.52288	5.83992	9.04258
O	8.19650	12.93618	3.06823
O	3.91480	7.82648	9.30086
O	5.67531	17.40586	3.10788
O	6.37004	3.33448	9.43082
Al	13.57220	1.62471	0.01837
Al	11.05355	6.18698	−0.03434
Al	13.63744	7.63464	0.03832
Al	11.02422	3.18583	−0.05474
Si	14.31392	0.04012	2.72217
Si	7.83560	−6.19015	9.64246
Si	11.74941	4.63342	2.68658
Si	10.53101	−1.70791	9.69736
Al	14.42912	3.05504	2.86125
Si	7.82213	−0.05368	9.66282
Si	11.93607	7.46705	2.68552
Si	10.29825	−4.63893	9.69384
O	14.17326	0.08998	1.10200
O	7.93397	−6.20581	11.27792
O	11.64757	4.67393	1.02411
O	10.52565	−1.73185	11.31318

Appendix 1. Continued.

Elem	X	Y	Z
O	14.51378	2.97112	1.04402
O	7.67253	0.03664	11.28530
O	12.03677	7.38250	1.07223
O	10.22284	−4.57126	11.29806
O	11.92851	1.84528	0.94143
O	10.30854	1.17943	11.44825
O	14.58641	6.23076	0.89319
O	7.72954	−3.24230	11.48644
H	12.13375	2.13609	1.85365
H	10.77209	2.06912	11.51427
H	14.15677	5.43265	0.57491
H	8.15808	−2.44447	11.78238
O	10.71891	3.59830	3.34933
O	11.61888	−0.74383	8.95307
O	13.27606	8.17359	3.39813
O	8.96748	−5.28775	8.89587
O	13.92316	1.50617	3.42176
O	8.05532	1.38024	9.01585
O	11.61407	6.11329	3.45857
O	10.64068	−3.19719	8.97020
O	13.23247	4.17931	3.00578
O	9.09425	−1.07688	9.36987
O	10.72838	8.49453	2.95741
O	11.49749	−5.67854	9.46331
Al	13.74804	10.64778	0.11501
Al	11.22328	15.15014	0.06631
Al	13.79004	16.64481	0.04428
Al	11.12873	12.15344	0.12323
Si	14.42155	9.07181	2.71314
Si	7.91549	2.85927	9.76572
Si	11.94814	13.57455	2.82111
Si	10.58568	7.31635	9.65091
Si	14.67048	11.97999	2.78806
Si	7.89348	8.89379	2.66861
Si	12.15484	16.51500	2.73082
Si	10.39046	4.43742	9.71894
O	14.32864	9.10490	1.07564
O	7.93815	2.81083	11.38045
O	11.82599	13.59405	1.11794
O	10.66225	7.27187	11.32243
O	14.70757	11.95254	1.11681
O	7.79753	8.98739	11.32762
O	12.20744	16.42048	1.08336
O	10.36535	4.45105	11.34726
O	12.06635	10.76645	1.02708
O	10.46851	10.18179	11.44713
O	14.67051	15.24684	0.95124
O	7.82407	5.68783	11.58591
H	11.55445	9.91620	0.84674
H	11.00393	10.99791	11.63724
H	14.18871	14.43792	0.87226
H	8.30794	6.50091	11.76737
O	10.71915	12.73768	3.57374
O	11.74055	8.20494	8.91867
O	13.39335	17.12308	3.51230
O	8.96916	3.82051	9.10151
O	14.36050	10.51470	3.43330
O	8.17809	10.34509	8.94517
O	11.87250	15.04628	3.48208
O	10.73140	5.81626	8.99507
O	13.43784	13.06230	3.08187
O	9.16947	7.95749	9.24584
O	10.89983	17.49197	2.96321
O	11.44417	3.29559	9.33848
Al	18.79284	1.59691	0.05717
Al	16.26181	6.13480	−0.00377

Appendix 1. Continued.

Elem	X	Y	Z
Al	18.86656	7.62210	0.04231
Al	16.17743	3.11549	0.01164
Si	19.45241	0.07467	2.78390
Si	12.97508	−6.27985	9.74962
Si	16.95198	4.59709	2.69129
Si	15.69721	−1.75827	9.62273
Si	19.66528	2.96108	2.70384
Si	12.96160	−0.21060	9.69760
Si	17.20190	7.48131	2.72961
Si	15.42894	−4.73800	9.65094
O	19.39695	0.11672	1.11482
O	13.12848	−6.28663	11.36326
O	16.80083	4.59712	1.06023
O	15.76646	−1.77503	11.26759
O	19.75533	2.90119	1.05772
O	12.90807	−0.05959	11.29291
O	17.21712	7.43825	1.08087
O	15.40274	−4.60908	11.29824
O	17.04234	1.71649	0.86825
O	15.52361	1.13826	11.48196
O	19.74945	6.19854	0.90463
O	12.88391	−3.32488	11.47915
H	16.50813	0.92234	0.63210
H	16.01159	1.95520	11.73437
H	19.22915	5.39473	0.80342
H	13.32041	−2.51573	11.68916
O	15.99147	3.52424	3.43590
O	16.81574	−0.81051	8.95948
O	18.55026	8.17194	3.48091
O	14.09887	−5.41616	8.91857
O	19.30998	1.50168	3.51644
O	13.39725	1.14261	8.91854
O	16.86248	6.03609	3.42760
O	15.74541	−3.27504	8.97703
O	18.54057	4.07463	2.98097
O	14.20523	−1.18880	9.36636
O	15.96710	8.50077	3.10353
O	16.68172	−5.75503	9.36069
Al	18.91981	10.62455	0.08337
Al	16.34044	15.11016	0.06962
Al	18.98147	16.62663	0.10300
Al	16.29829	12.13894	0.06794
Si	19.54963	9.15789	2.75486
Al	13.08989	2.79420	9.49864
Al	17.10813	13.58602	2.91277
Si	15.80476	7.34270	9.75309
Si	19.87022	12.05678	2.79347
Si	13.02047	8.84328	9.75288
Si	17.21754	16.57292	2.76869
Si	15.59468	4.44978	9.72320
O	19.45629	9.10526	1.10674
O	13.28908	2.76138	11.32053
O	16.95023	13.61277	1.08739
O	15.87693	7.28964	11.41728
O	19.89610	11.95132	1.14481
O	12.97593	8.95838	11.39586
O	17.28952	16.44225	1.11864
O	15.52980	4.48271	11.36589
O	17.23831	10.71507	1.01160
O	15.67984	10.17351	11.55162
O	19.86785	15.22614	1.04964
O	12.99908	5.71063	11.51818
H	16.75297	9.85766	0.92836
H	16.15453	10.97642	11.65050
H	19.34021	14.41273	0.90190
H	13.44142	6.57903	11.67661

Appendix 1. Continued.

Elem	X	Y	Z
O	16.00686	12.37315	3.50117
O	16.81046	8.39228	8.99770
O	18.58214	17.12081	3.45886
O	14.24513	3.97363	8.92387
O	19.40537	10.66438	3.54618
O	13.22133	10.26829	8.98387
O	16.64084	15.22507	3.46303
O	16.02050	5.87984	9.02185
O	18.78912	13.20300	3.11864
O	14.26973	7.82835	9.45903
O	16.03030	17.68487	3.00266
O	16.75549	3.37715	9.29899
Ca	0.13840	10.65758	7.26322
N	0.96743	2.75004	6.21484
C	−2.79782	2.63709	6.13131
H	−3.60893	1.94472	6.29765
C	−1.45831	2.19678	6.19927
H	−1.22821	1.08092	6.37244
C	−0.43912	3.14189	6.19498
C	−0.83491	4.47228	6.09482
H	−0.08571	5.25282	6.14642
C	−2.18259	4.89026	6.06801
C	−3.19883	3.97711	6.08401
S	−2.52996	6.63112	6.25086
C	−4.25257	6.63067	6.22064
C	−5.06970	5.48691	6.21485
N	−4.57782	4.12144	6.17936
C	−4.83629	7.88219	6.18938
H	−4.15322	8.77368	6.13436
C	−6.21066	8.06131	6.26430
C	−6.99075	6.92419	6.29063
H	−8.08675	6.98593	6.19597
C	−6.42389	5.63196	6.19835
H	−7.13310	4.86403	6.23631
N	−6.67712	9.48629	6.26798
C	−5.72625	10.66382	6.46510
H	−4.96024	10.77737	5.67270
H	−6.33161	11.58270	6.40142
H	−5.30272	10.64414	7.45741
C	−8.11581	9.84444	6.18057
H	−8.78957	9.07912	6.47076
H	−8.47092	10.69869	6.69792
H	−8.37301	10.04623	5.07984
C	2.09408	3.75884	6.34275
H	3.11431	3.30084	6.29701
H	2.05728	4.50397	5.53568
H	2.11267	4.40739	7.26109
C	1.34913	1.36244	5.93385
H	1.10918	1.00377	4.95835
H	2.44153	1.33105	5.91943
H	1.01229	0.80814	6.75107
N	6.16360	7.53441	6.13170
C	9.40842	5.58761	6.14158
H	10.51611	5.68987	6.03356
C	8.48037	6.66848	6.17296
H	8.88131	7.68488	6.31109
C	7.10355	6.45062	6.26404
C	6.66934	5.15295	6.26996
H	5.55178	4.91211	6.08233
C	7.52722	4.08140	6.14619
C	8.88228	4.31318	6.10158
S	6.87184	2.53612	6.08248
C	8.27144	1.56642	6.19522
C	9.53972	2.08750	6.16549
N	9.87008	3.39242	6.15642
H	8.01213	0.19074	6.15672

Appendix 1. Continued.

Elem	X	Y	Z
C	6.98697	−0.08796	6.07899
C	9.11389	−0.73753	6.19680
C	10.42849	−0.15600	6.24701
H	11.35506	−0.82093	6.22711
C	10.57945	1.21223	6.32769
H	11.55818	1.68231	6.51973
N	8.8261	−2.09080	6.30232
C	9.80168	−3.16722	5.95903
H	9.76629	−4.12455	6.51994
H	9.43638	−3.39385	4.93163
H	10.85107	−2.83239	5.86340
C	7.49977	−2.66291	6.56392
H	7.50546	−3.17158	7.49412
H	6.66377	−1.93131	6.48475
H	7.25277	−3.44276	5.84435
C	4.67781	7.32012	5.91607
H	4.52793	6.78165	4.98191
H	4.28028	6.67108	6.72680
H	4.04877	8.30499	5.93725
C	6.48015	8.94929	6.15849
H	7.57248	9.23861	6.13206
H	6.11769	9.53688	5.20864
H	6.04106	9.52027	7.04272
Ca	14.64461	2.37717	6.55618

[1] For a definition of the model see the text. The atomic coordinates are given in cols. X, Y, Z. Element symbols are given in col. Elem. The number of significant figures is not representative of the accuracy of the modeled results and given here for adequate computations of atom positions. The unit cell constants are a = 20.73 Å, b = 18.03 Å, c = 14.74 Å, α = 115.85°, β = 109.84°, and γ = 89.28°.

Appendix 2. Atomic Cartesian coordinates (Å) for model beid421-2MB-106w.[1]

Elem	X	Y	Z
Al	2.33452	1.39730	−0.04883
Al	−0.24496	5.91301	−0.01181
Al	2.36017	7.36836	0.00731
Al	−0.28978	2.91524	−0.05853
Si	2.96700	−0.10176	2.67620
Si	0.32921	−9.32504	14.92679
Si	0.45415	4.35803	2.64060
Si	3.01161	−4.69989	14.94484
Si	3.16057	2.79573	2.66123
Si	0.23292	−3.16955	14.96394
Al	0.62605	7.35135	2.80303
Al	2.84170	−7.72742	14.80631
O	2.92856	−0.12724	1.05216
O	0.42323	−9.29833	16.55470
O	0.38114	4.39325	0.97916
O	3.09334	−4.73658	16.59615
O	3.25290	2.67707	1.01924
O	0.19191	−3.11380	16.60795

https://doi.org/10.1346/CCMN.2000.0480608 Published online by Cambridge University Press

Appendix 2. Continued.

Elem	X	Y	Z
O	0.71283	7.22675	1.00813
O	2.74389	−7.61448	16.61962
O	0.64163	1.51885	0.83554
O	2.75814	−1.93095	16.71030
O	3.28768	5.98289	0.92117
O	0.18216	−6.38498	16.74555
H	0.20257	0.67916	0.71309
H	3.22543	−1.11236	16.73068
H	2.81719	5.20228	0.85303
H	0.62967	−5.52256	16.92847
O	−0.61945	3.32665	3.33256
O	4.05172	−3.65094	14.24617
O	2.14857	7.89253	3.44092
O	1.25731	−8.24731	14.22869
O	2.93711	1.37311	3.39273
O	0.39337	−1.74188	14.23958
O	0.11270	5.77708	3.37162
O	3.27797	−6.13949	14.25755
O	1.96788	3.77643	3.00701
O	1.50789	−4.16045	14.54229
O	−0.61111	8.54544	2.98262
O	4.07051	−8.92572	14.53750
Al	2.41718	10.42964	0.03960
Al	−0.16978	14.93701	−0.01454
Al	2.42936	16.45356	−0.01294
Al	−0.24310	11.93716	−0.02563
Si	3.13944	8.87683	2.67506
Si	0.32258	−0.27172	15.01871
Si	0.63809	13.42727	2.59875
Al	3.04411	4.27443	14.85447
Si	3.28070	11.80285	2.67204
Si	0.25897	5.87998	14.93056
Si	0.73908	16.36042	2.68600
Si	2.79827	1.28098	14.97988
O	3.06299	8.87704	1.07137
O	0.53801	−0.26990	16.66105
O	0.50438	13.43200	0.99441
O	3.16048	4.28256	16.61446
O	3.38921	11.73619	1.08724
O	0.24429	5.95407	16.59569
O	0.81803	16.20988	1.02786
O	2.75735	1.41089	16.65559
O	0.72849	10.54575	0.92941
O	2.85943	7.14001	16.75446
O	3.36739	14.96751	0.84494
O	0.20904	2.68587	16.81632
H	0.27527	9.66505	0.88397
H	3.36955	7.96686	16.83517
H	2.92586	14.15078	0.54710
H	0.64589	3.54298	16.92700
O	−0.48430	12.47596	3.36820
O	4.20494	5.38907	14.14448
O	2.00957	17.02967	3.42178
O	1.42412	0.66654	14.29742
O	3.20234	10.35775	3.44228
O	0.72466	7.24236	14.18313
O	0.49609	14.91478	3.41388
O	3.32309	2.66614	14.35793
O	2.06766	12.79103	2.95718
O	1.38083	4.75678	14.62821
O	−0.43355	17.41557	2.94981
O	4.02446	0.21558	14.63444
Al	7.54160	1.37882	−0.07203
Al	4.96912	5.91378	0.01050
Al	7.52618	7.43007	0.00769
Al	4.87327	2.91412	−0.04945

Appendix 2. Continued.

Elem	X	Y	Z
Si	8.26774	−0.11242	2.60017
Si	5.57116	−9.32664	14.95345
Si	5.62171	4.38298	2.69726
Si	8.13697	−4.68922	14.92989
Si	8.38164	2.76776	2.60801
Si	5.41571	−3.10232	14.96638
Si	5.84189	7.35511	2.67499
Si	7.89602	−7.62856	14.89757
O	8.13307	−0.10149	0.95987
O	5.65446	−9.30707	16.56978
O	5.54853	4.35848	1.03627
O	8.22850	−4.73949	16.59698
O	8.45738	2.70403	0.96277
O	5.33544	−3.08095	16.59739
O	5.91679	7.22303	1.03866
O	7.88514	−7.54593	16.52434
O	5.85298	1.54143	0.85413
O	8.00776	−1.84412	16.70107
O	8.43758	6.01886	0.92730
O	5.32730	−6.43147	16.71014
H	5.39827	0.67133	0.84674
H	8.44847	−0.98099	16.83466
H	7.99046	5.17456	1.03527
H	5.86243	−5.60613	16.80740
O	4.54001	3.41856	3.45964
O	9.28807	−3.76854	14.18906
O	7.20541	7.97527	3.39412
O	6.61932	−8.33419	14.20183
O	8.11892	1.34365	3.30510
O	5.72722	−1.70189	14.20480
O	5.55995	5.91075	3.36298
O	8.11062	−6.11270	14.23407
O	7.09526	3.77392	2.95754
O	6.66320	−4.02439	14.57656
O	4.65152	8.35254	3.05550
O	9.27623	−8.51362	14.58120
Al	7.54979	10.46262	0.00548
Al	5.05017	14.96169	−0.00997
Al	7.61391	16.43305	0.00254
Al	4.96666	11.95926	0.02218
Si	8.24469	8.93053	2.69052
Si	5.55622	−0.23764	14.98153
Si	5.70550	13.44624	2.71218
Si	8.21639	4.28274	14.98471
Si	8.47790	11.87079	2.71859
Si	5.51804	5.83635	15.02352
Si	5.90230	16.40094	2.70184
Si	7.98727	1.35391	15.01839
O	8.18283	8.91711	1.07206
O	5.69026	−0.24398	16.60861
O	5.61514	13.45789	1.05015
O	8.34897	4.27809	16.63244
O	8.50675	11.77784	1.07897
O	5.44395	5.94311	16.64209
O	6.00406	16.25104	1.04708
O	7.92996	1.44547	16.63490
O	5.90961	10.59430	0.90660
O	8.03884	7.10210	16.73283
O	8.56801	15.06365	0.90888
O	5.43047	2.68963	16.79875
H	5.42365	9.77663	0.75761
H	8.58540	7.90420	16.80916
H	8.06348	14.22713	0.69004
H	5.94348	3.51981	16.91685
O	4.65716	12.46768	3.38417
O	9.32205	5.23481	14.26782

Appendix 2. Continued.

Elem	X	Y	Z
O	7.31275	16.92344	3.37231
O	6.64306	0.76094	14.27890
O	8.31498	10.42643	3.42094
O	5.95556	7.21112	14.27174
O	5.56100	14.97251	3.40892
O	8.39167	2.79698	14.28096
O	7.17600	12.83833	2.99066
O	6.66611	4.73231	14.74586
O	4.69788	17.41714	3.01026
O	9.24909	0.35220	14.77133
Al	12.70943	1.43190	−0.00735
Al	10.13321	5.93907	−0.05251
Al	12.73172	7.42140	−0.01907
Al	10.08832	2.91991	−0.03246
Si	13.44716	−0.14350	2.64194
Si	10.69141	−9.23550	14.97901
Si	10.79743	4.41862	2.65867
Si	13.33551	−4.67941	14.92345
Al	13.53099	2.88793	2.75887
Si	10.58286	−3.10748	14.90808
Si	10.97509	7.35835	2.56998
Si	13.16765	−7.61193	14.94147
O	13.28926	−0.03968	1.03189
O	10.76464	−9.23506	16.62284
O	10.72685	4.39683	1.01349
O	13.43706	−4.72010	16.58924
O	13.66801	2.80467	0.97164
O	10.50986	−3.04631	16.54088
O	11.11001	7.26292	0.97387
O	13.09236	−7.56277	16.60163
O	10.99548	1.50274	0.85307
O	13.16743	−1.83021	16.76684
O	13.65347	6.05138	0.89783
O	10.55351	−6.28285	16.78257
H	10.52100	0.65676	0.76897
H	13.58137	−0.94333	16.85270
H	13.20467	5.21665	0.68090
H	11.03646	−5.47798	17.00770
O	9.64796	3.50070	3.37397
O	14.46126	−3.75787	14.24460
O	12.28401	7.95871	3.28313
O	11.88709	−8.34007	14.25363
O	13.15291	1.26647	3.36794
O	10.81341	−1.61770	14.22118
O	10.55114	5.91872	3.32417
O	13.39853	−6.17724	14.18437
O	12.29122	4.01264	2.95149
O	11.83595	−4.09281	14.62376
O	9.77877	8.39063	2.91297
O	14.46865	−8.59076	14.65250
Al	12.74086	10.44039	0.00472
Al	10.21640	14.96225	0.00037
Al	12.80851	16.49801	−0.00711
Al	10.15346	11.96310	0.02106
Si	13.47734	8.92041	2.65366
Si	10.79538	−0.22196	15.00239
Si	10.88575	13.40595	2.69292
Si	13.39590	4.29279	14.96104
Si	13.65159	11.76216	2.66484
Si	10.66673	5.93754	14.92873
Si	11.15740	16.34461	2.68800
Si	13.19818	1.40708	14.93494
O	13.39085	8.91348	0.99954
O	10.81495	−0.23492	16.64621
O	10.83979	13.44831	1.05314
O	13.40812	4.28463	16.60321

Appendix 2. Continued.

Elem	X	Y	Z
O	13.72715	11.77449	1.00715
O	10.60905	5.98372	16.58964
O	11.16903	16.25352	1.03622
O	13.13752	1.42848	16.57396
O	11.08573	10.57120	0.94360
O	13.26845	7.22685	16.77485
O	13.73866	15.07791	0.86352
O	10.64209	2.70924	16.76680
H	10.62210	9.71561	0.89628
H	13.77703	8.02363	16.97652
H	13.29009	14.16667	0.78650
H	11.17968	3.49951	16.91275
O	9.75822	12.55332	3.39775
O	14.51342	5.21161	14.21283
O	12.58520	16.81994	3.36864
O	11.77508	0.83113	14.20615
O	13.28093	10.38258	3.43922
O	10.85607	7.36141	14.21154
O	10.82963	14.95492	3.36027
O	13.58745	2.82022	14.21881
O	12.40164	12.86649	2.94704
O	11.92436	4.86531	14.61303
O	9.94941	17.44695	3.01846
O	14.26201	0.28458	124.60963
Al	17.85260	1.36711	−0.06533
Al	15.33115	5.95160	−0.00752
Al	17.93113	7.46433	−0.02081
Al	15.29610	2.95393	−0.03126
Si	18.63731	−0.08325	2.69366
Si	15.87599	−9.30474	14.91688
Si	16.17843	4.38232	2.64119
Si	18.57720	−4.73590	14.95870
Si	18.81825	2.76908	2.61742
Si	15.79624	−3.20022	14.96837
Si	16.21356	7.36284	2.67934
Si	18.32094	−7.69747	14.88610
O	18.50357	−0.06461	1.03151
O	15.97856	−9.25362	16.54017
O	16.01243	4.42407	0.97496
O	18.61736	−4.75180	16.59842
O	18.84286	2.70870	0.97309
O	15.68922	−3.01822	16.56684
O	16.26374	7.27687	1.04014
O	18.24426	−7.61525	16.55882
O	16.17773	1.51714	0.82105
O	18.33662	−1.86597	16.74937
O	18.85262	6.02500	0.85989
O	15.69227	−6.43380	16.67896
H	15.68200	0.71341	0.66766
H	18.76822	−1.02364	16.81737
H	18.46497	5.13081	0.87080
H	16.15091	−5.58612	16.74151
O	15.04725	3.45852	3.38070
O	19.67773	−3.78259	14.22150
O	17.54605	7.96998	3.41029
O	16.99489	−8.35295	14.17624
O	18.45039	1.35075	3.33573
O	16.21686	−1.87294	14.33059
O	15.97812	5.89195	3.32889
O	18.65262	−6.23203	14.23803
O	17.61338	3.86588	2.93369
O	17.06826	−4.19056	14.68630
O	14.94852	8.28874	3.11313
O	19.52106	−8.82183	14.54425
Al	17.92732	10.48835	−0.01552
Al	15.38037	14.95505	−0.03289

https://doi.org/10.1346/CCMN.2000.0480608 Published online by Cambridge University Press

Appendix 2. Continued.

Elem	X	Y	Z
Al	17.99145	16.48754	−0.03611
Al	15.33762	11.92908	−0.02826
Si	18.61500	8.96293	2.67493
Al	15.90914	−0.20410	14.85918
Al	16.16893	13.43088	2.77435
Si	18.62534	4.31994	14.95148
Si	18.91488	11.85237	2.75086
Si	15.85434	5.81569	14.95001
Si	16.32746	16.34877	2.62877
Si	18.42328	1.41859	14.96445
O	18.51924	9.00584	1.07443
O	16.03348	−0.19994	16.65693
O	15.97913	13.44630	0.98194
O	18.67522	4.31657	16.59182
O	18.95143	11.78289	1.08357
O	15.78417	5.89613	16.57766
O	16.40374	16.26384	0.97845
O	18.28386	1.52951	16.56590
O	16.26699	10.51830	0.81259
O	18.46070	7.19820	16.80100
O	18.90633	15.06652	0.89412
O	15.75328	2.67891	16.75140
H	15.75725	9.75068	0.53495
H	19.01018	8.01841	16.88148
H	18.32570	14.25894	0.91500
H	16.17876	3.54428	16.92352
O	15.04353	12.20421	3.39753
O	19.63583	5.34222	14.20206
O	17.69765	16.9407	3.37348
O	17.05760	0.94399	14.26640
O	18.45346	10.46323	3.44327
O	16.13534	7.27531	14.22772
O	15.76777	15.05100	3.37531
O	18.71555	2.87438	14.18755
O	17.81456	12.98127	3.04116
O	17.13277	4.85560	14.63135
O	15.19980	17.51250	2.91830
O	19.60256	0.35768	14.69112
Ca	10.66337	8.72715	7.57488
N	4.27891	−5.99976	11.27268
C	2.60225	−3.78362	8.89409
H	1.78566	−3.93756	8.17796
C	2.83683	−4.83089	9.71454
H	2.29820	−5.78928	9.72631
C	3.90937	−4.79944	10.60935
C	4.65885	−3.63513	10.74499
H	5.34336	−3.51224	11.56876
C	4.45002	−2.55897	9.86318
C	3.39252	−2.66295	8.93783
S	5.34608	−1.09666	10.00660
C	4.68596	−0.12209	8.80989
C	3.69622	−0.58504	7.84585
N	3.09282	−1.78411	7.89189
C	5.18255	1.13843	8.67660
H	5.68879	1.51951	9.55313
C	4.75383	2.02143	7.71894
C	3.87758	1.49037	6.75363
H	3.53253	2.08299	5.94128
C	3.25863	0.21191	6.81426
H	2.42421	−0.10636	6.12181
N	5.19905	3.36523	7.70235
C	4.99927	4.24164	6.53270
H	5.83767	4.15291	5.84387
H	4.06682	3.98597	6.09301
H	4.70648	5.23822	6.81063
C	6.27773	3.74757	8.63457
H	7.08670	3.07686	8.75770

Appendix 2. Continued.

Elem	X	Y	Z
H	6.82431	4.68346	8.36634
H	5.71740	3.98048	9.52660
C	5.64182	−6.13436	11.94681
H	6.32537	−5.44675	11.38844
H	5.59329	−5.83153	13.00417
H	6.09827	−7.06195	11.75364
C	3.48484	−7.14279	11.27570
H	3.84413	−7.80538	12.03196
H	2.38925	−6.96882	11.56631
H	3.50579	−7.77216	10.42896
N	15.87090	13.01218	7.90783
C	18.78122	11.04667	6.54491
H	19.52433	11.19483	5.75021
C	17.90290	12.07846	6.73451
H	17.87117	12.96066	6.15901
C	16.91122	11.99398	7.70137
C	16.87067	10.88814	8.55331
H	16.10754	10.70586	9.28960
C	17.80542	9.85168	8.27714
C	18.77929	9.90909	7.32258
S	17.55390	8.39837	9.16685
C	18.73041	7.37503	8.53164
C	19.62844	7.79802	7.53333
N	19.65163	8.95279	6.92697
C	18.81338	6.11171	9.10338
H	17.96917	5.79457	9.61987
C	19.82919	5.24163	8.72390
C	20.62887	5.68050	7.59895
H	21.28095	4.98760	7.11834
C	20.60914	6.96060	7.13420
H	21.25342	7.31329	6.32474
N	20.09440	3.96492	9.32784
C	21.20357	3.08525	8.88289
H	22.08006	3.67290	8.58220
H	21.47729	2.31467	9.64601
H	20.80389	2.55463	7.99719
C	19.40939	3.67647	10.58174
H	19.92271	4.19140	11.46089
H	18.43424	4.06307	10.55535
H	19.38228	2.56197	10.69590
C	14.88966	12.97293	9.06674
H	14.17457	13.77866	9.02917
H	14.28375	12.06272	9.06250
H	15.45120	13.01233	9.98005
C	15.87577	14.30332	7.18068
H	15.30836	15.02945	7.77625
H	16.90293	14.61080	7.23803
H	15.70590	14.11351	6.10891
Ca	19.32444	−1.01310	10.30116
O	10.90536	10.35725	5.53757
H	10.06878	10.47629	4.97768
H	11.16223	11.32537	5.76680
O	13.55486	5.42858	7.85545
H	13.35699	4.50881	7.89256
H	13.56882	5.60614	6.85698
O	18.60639	3.24857	6.01418
H	19.54975	3.24901	6.25910
H	18.54126	4.18254	5.64894
O	7.80620	15.63531	8.38808
H	8.77153	15.76845	8.46059
H	7.66310	14.72051	8.79830
O	15.67887	8.00309	6.96091
H	16.15457	8.59121	6.34886
H	14.88620	7.95708	6.45149
O	8.48726	14.56558	5.64058
H	9.01396	15.45173	5.57536
H	7.59598	15.02348	5.66826

Appendix 2. Continued.

Elem	X	Y	Z
O	9.26605	17.01648	6.09308
H	8.80843	17.51421	6.78372
H	10.05213	17.62036	5.98729
O	8.78829	7.47685	9.06188
H	9.28853	6.59746	9.19500
H	8.34768	7.46617	9.93650
O	12.81113	8.29121	6.25024
H	13.11302	7.54215	5.62885
H	12.67974	9.05361	5.59902
O	9.42805	4.12564	8.94184
H	10.10452	3.46024	8.81944
H	9.04758	4.08575	8.02367
O	16.57304	5.32054	6.76684
H	16.32916	6.20944	7.07712
H	17.34532	5.66648	6.25595
O	0.87822	10.12610	5.46463
H	0.13931	9.63537	5.94990
H	0.60614	9.81860	4.54028
O	13.61634	11.39617	6.34326
H	14.42704	10.94812	6.00481
H	13.60803	12.16957	5.75517
O	2.71271	23.99418	5.67051
H	2.00001	23.80244	5.08578
H	3.09432	24.79736	5.24716
O	14.03359	2.93178	6.25220
H	14.75523	2.22940	6.30308
H	14.33431	3.46489	5.46575
O	10.44521	16.27077	9.03156
H	10.28709	17.08219	9.63855
H	11.34454	16.51137	8.73604
O	8.34897	9.23819	6.56197
H	8.23493	10.22016	6.38322
H	7.39291	8.92380	6.63411
O	9.48702	10.79590	8.61588
H	10.10427	11.55272	8.64742
H	8.61556	11.28617	8.83271
O	5.78249	−2.11536	6.43784
H	6.10045	−2.34104	7.35699
H	6.17737	−1.21280	6.26452
O	15.18905	−1.03736	5.81200
H	15.42765	−1.63050	5.03773
H	15.46895	−0.182127	5.45055
O	12.97923	2.77166	8.55177
H	12.13567	2.31276	8.72315
H	13.08979	2.57917	7.61491
O	16.47338	1.56407	5.76305
H	17.37522	1.88595	6.00142
H	16.47125	1.71944	4.78637
O	−2.14528	5.82986	5.18193
H	−2.06456	6.41849	4.33878
H	−1.17661	5.55481	5.19751
O	15.97771	10.35170	5.43141
H	15.92946	11.04949	4.67212
H	16.92813	10.16254	5.30401
O	10.51958	1.62297	8.24088
H	9.64989	1.23455	8.62323
H	11.00213	1.00521	7.61849
O	8.67321	13.95703	11.03272
H	9.35694	13.56341	11.64955
H	8.46058	13.18878	10.47953
O	6.01488	7.60948	6.48067
H	5.95507	7.36165	7.49804
H	5.01856	7.87190	6.36935
O	−2.71486	−0.99796	6.64311
H	−2.50641	−1.91186	6.31651
H	−3.69780	−1.04503	6.50648
O	3.31860	8.61510	6.35177

Appendix 2. Continued.

Elem	X	Y	Z
H	2.71701	9.00880	5.68787
H	2.91298	8.92447	7.18204
O	5.62378	10.45089	5.31278
H	5.02539	9.77128	4.95415
H	5.20080	11.33546	5.04940
O	16.49223	5.83336	11.51046
H	15.82095	6.28789	10.89532
H	15.86788	5.64812	12.25767
O	13.51430	5.76693	5.04834
H	13.02458	5.41555	4.31358
H	14.38709	5.55991	4.61474
O	11.43861	21.99973	6.00125
H	11.14581	21.12323	5.60528
H	12.36849	21.78113	6.11732
O	13.30842	14.86428	5.48514
H	12.82737	15.69617	5.24402
H	13.76442	14.73082	4.63634
O	0.01535	18.55105	5.75416
H	0.27097	17.60116	5.89442
H	−0.94445	18.39813	5.91898
O	35.66589	−8.88458	11.27420
H	35.33140	−9.52972	11.95477
H	35.72225	−9.60135	10.60133
O	0.51295	−2.26184	6.26500
H	1.30817	−2.48074	5.72150
H	0.30991	−3.18048	6.43214
O	−2.23037	−3.18579	5.38376
H	−2.69479	−3.49232	4.60886
H	−1.30096	−3.20353	5.02222
O	6.63216	18.57234	5.83926
H	7.36078	18.65937	5.17384
H	6.31023	19.47627	5.97812
O	10.33905	6.35873	6.41395
H	10.92586	5.57000	6.30491
H	9.64623	6.19019	5.76498
O	5.76465	13.30979	6.27678
H	5.68432	14.29282	6.46770
H	4.85740	13.04540	6.27219
O	14.91688	7.06818	9.49570
H	14.29719	6.43316	9.01318
H	15.35090	7.48990	8.72078
O	18.83415	−3.22151	9.25333
H	18.54809	−3.92832	9.86400
H	18.84627	−3.80764	8.48417
O	0.97034	2.82083	5.93487
H	0.87441	2.69452	4.95951
H	0.85161	1.87720	6.13149
O	8.59174	21.08183	6.31745
H	9.22667	21.77633	6.02487
H	9.09799	20.27980	6.19612
O	15.68027	−6.34406	12.10021
H	15.58005	−7.28302	11.79251
H	15.17204	−6.40253	12.90201
O	13.70004	4.21791	10.99094
H	14.38541	3.60776	11.27372
H	13.51345	3.88518	10.07572
O	11.99261	25.36460	9.15998
H	11.83154	24.73681	9.96452
H	12.78458	24.87040	8.82486
O	0.26267	13.16130	6.84361
H	0.03106	12.46014	6.20111
H	0.27236	12.61230	7.68226
O	11.05257	1.37210	5.24305
H	11.68354	0.92630	5.86118
H	11.60154	1.29196	4.43678
O	13.09850	−1.41615	8.99543
H	14.04655	−1.25156	8.78169

https://doi.org/10.1346/CCMN.2000.0480608 Published online by Cambridge University Press

Appendix 2. Continued.

Elem	X	Y	Z
H	13.28112	−1.42581	9.95873
O	3.27378	14.98850	5.48792
H	4.18456	14.74918	5.45198
H	3.30372	15.70282	6.15718
O	12.20901	−4.05592	11.34727
H	11.74806	−4.82944	11.70211
H	11.67023	−3.86125	10.56116
O	17.74410	−4.99685	11.08783
H	18.48180	−5.63507	11.35827
H	16.96061	−5.43700	11.49106
O	8.31346	0.03877	8.73203
H	7.83997	0.65017	9.57489
H	7.93290	−0.53089	8.57778
O	1.84249	9.58198	8.49848
H	1.01242	10.10212	8.46511
H	1.59496	9.21667	8.38330
O	11.33661	13.21713	6.49962
H	10.53441	13.54128	5.93081
H	12.02447	13.86927	6.39074
O	11.04077	5.62682	11.20220
H	11.81154	4.94506	11.33947
H	10.41321	4.86839	11.10135
O	21.79500	2.76051	12.16092
H	22.05445	3.71123	11.92300
H	22.13935	2.65084	13.06077
H	10.53952	13.33815	9.05672
H	10.12157	14.20403	9.29949
O	10.91517	13.47328	8.12709
O	15.13119	0.71665	8.67872
H	15.95958	1.17871	8.35849
H	14.55806	1.51765	8.70022
O	16.81564	−1.16060	9.81230
H	16.14018	−0.47178	9.49891
H	16.22580	−1.77323	10.34629
O	7.36342	12.62896	8.69374
H	6.45881	12.23206	8.77772
H	7.40304	12.62592	7.73178
O	21.63948	−9.613760	11.03262
H	21.12195	−10.36623	11.34321
H	22.49480	−9.81435	11.53784
O	−0.23315	−6.44825	9.06075
H	−0.95074	−7.01579	9.48547
H	0.16141	−6.11207	9.92155
O	18.38601	−2.00199	12.34330
H	19.06459	−2.65650	12.74549
H	17.58660	−1.99693	13.06305
O	10.62863	8.77864	11.52872
H	9.67194	8.72139	11.85075
H	10.81939	7.80288	11.47799
O	8.17337	22.46796	11.57294
H	8.59784	21.94439	10.83894
H	8.66062	22.02732	12.35903
O	7.94704	−1.37017	11.92897
H	7.14225	−1.42249	12.52766
H	8.07472	−2.32695	11.91281
O	8.19882	7.35126	11.81725
H	7.31676	7.39335	12.25397
H	8.60636	6.58722	12.20365
O	3.29867	3.35901	10.22404
H	3.10784	3.50038	9.28529
H	3.09905	4.26443	10.60101
O	10.55811	−15.39633	11.55300
H	10.67127	−15.89317	12.45951
H	9.98815	−16.05614	11.08390
O	17.89460	0.88835	11.41056
H	17.69368	0.53854	12.31029

Appendix 2. Continued.

Elem	X	Y	Z
H	17.35177	1.70431	11.26250
O	8.10274	11.85852	6.14953
H	7.19888	11.87635	5.77326
H	8.32849	12.78722	5.94111
O	13.50735	1.10137	11.27665
H	13.68597	0.23845	11.73148
H	12.65237	1.41541	11.60972
O	6.31917	9.05023	10.02299
H	5.85640	9.67553	9.35872
H	5.91211	8.21905	9.76915
O	12.84928	17.75280	6.68788
H	12.90404	17.23449	7.53781
H	13.71879	17.50268	6.25099
O	23.76768	−5.81139	6.37898
H	22.94218	−5.34747	6.15425
H	23.44937	−6.71020	6.06707
O	4.87104	−11.17329	9.13659
H	5.14470	−11.67508	9.90773
H	3.90435	−11.14904	9.25331
O	5.36747	2.30490	11.88162
H	5.08614	2.99510	11.24136
H	4.96503	2.69205	12.68901
O	5.38462	−12.45536	11.37817
H	5.06794	−12.33578	12.26926
H	6.34897	−12.63244	11.42508
O	7.89470	5.74533	5.42736
H	7.55706	6.29526	4.65267
H	7.64023	6.33852	6.17673
O	4.97325	−7.43379	8.06737
H	5.22093	−7.82325	7.23885
H	4.10467	−7.09628	7.77440
O	19.08528	−7.84510	11.48297
H	18.31387	−8.40483	11.70576
H	19.68965	−8.61864	11.45869
O	2.59105	−2.04831	12.04584
H	3.13281	−2.72404	12.52947
H	2.87545	−1.19269	12.39383
O	21.01101	−2.89551	11.22637
H	21.01556	−3.84426	11.28116
H	21.76319	−2.67276	11.80348
O	21.19168	−5.36226	11.87877
H	21.78953	−5.18065	12.63611
H	20.61542	−6.11092	12.21548
O	10.56123	−0.11403	11.20368
H	11.46975	−0.55228	11.31428
H	10.07738	−0.75071	11.85168
O	16.93024	2.95361	8.20943
H	17.32302	3.30473	7.27399
H	16.24994	3.68132	8.32357
O	8.53762	10.46874	11.32857
H	8.92402	10.29013	10.48583
H	7.81662	9.82020	11.31909
O	12.85443	−1.53538	11.91554
H	13.29092	−1.52888	12.79485
H	12.74177	−2.51896	11.72901
O	21.49160	−0.75119	9.01775
H	22.13076	−0.73440	8.19408
H	22.17639	−1.11168	9.63460
O	13.25070	7.27751	12.33879
H	13.23709	6.32253	12.30068
H	12.35299	7.52985	12.58126
O	10.63949	11.98219	12.04361
H	11.50042	11.62491	11.81791
H	10.16527	11.14323	12.26561
O	18.96579	18.87311	8.45647
H	18.69013	18.25164	7.77439

Appendix 2. Continued.

Elem	X	Y	Z
H	18.40308	19.69507	8.34994
O	3.30169	0.77564	11.56394
H	3.00634	1.66593	11.30573
H	4.15689	1.02139	11.98886
O	22.66205	5.23664	11.53768
H	23.06797	6.03531	11.18419
H	22.35745	5.52959	12.48577
O	0.24883	0.26340	11.56755
H	1.10054	−0.10885	11.86219
H	0.40922	1.19343	11.74478
O	15.74582	2.63847	12.07494
H	15.01851	2.02613	12.01267
H	16.20574	2.18377	12.84964
O	12.62917	10.55339	11.03511
H	13.48213	10.04279	11.13037
H	12.05567	9.73391	11.07026
O	7.79342	1.34452	11.08833
H	6.99045	1.65348	11.46396
H	7.95642	0.50109	11.49326
O	12.38361	10.16689	8.48046
H	13.07768	10.50191	7.86672
H	12.54728	10.55278	9.38478
O	−18.11165	5.85473	8.41018
H	−17.78827	5.69834	7.51885
H	−18.93752	6.37404	8.26110
O	18.50187	−10.65146	12.15686
H	17.81088	−11.15166	11.69983
H	18.73702	−11.26100	12.84804
O	15.49027	−2.77595	11.32596
H	15.93993	−3.15882	12.04881
H	14.55187	−3.18573	11.39596
O	3.20682	7.62801	12.38248
H	3.36114	8.36874	13.05245
H	3.49725	6.83342	12.86068

[1] For a definition of the model see the text. The atomic coordinates are given in cols. X, Y, Z. Element symbols are given in col. Elem. The number of significant figures is not representative of the accuracy of the modeled results and given for adequate computations of atom positions. The unit cell constants are a = 20.76 Å, b = 18.05 Å, c = 19.94 Å, α = 117.49°, β = 93.56°, and γ = 89.50°.

https://doi.org/10.1346/CCMN.2000.0480608 Published online by Cambridge University Press